

Behavior of Deep Convective Clouds in the Tropical Pacific Deduced from ISCCP Radiances

RONG FU

Department of Geological Sciences, Columbia University, New York, New York

ANTHONY D. DEL GENIO AND WILLIAM B. ROSSOW

NASA/Goddard Space Flight Center, Institute for Space Studies, New York, New York

(Manuscript received 8 August 1989, in final form 25 April 1990)

ABSTRACT

We analyze the properties of deep convection over the equatorial Pacific and its relationship to sea surface temperature (SST) and surface wind divergence using ISCCP radiance data for July 1983 and January 1984. Deep convective clouds (DCC) are diagnosed with both a combined visible-infrared threshold method and an infrared-only threshold method. The visible channel is important in diagnosing deep convection in different regions with different surface and atmospheric properties because of the existence of large-scale variations of DCC top altitudes.

The ITCZ and SPCZ exhibit changes in these two months that are characteristic of both the El Niño and seasonal cycles. Deep convection is latitudinally confined to a much smaller spatial scale than that suggested by maps of outgoing longwave radiation. Diurnal variations of DCC cover and associated mesoscale cirrus/anvil cloud (CAC) cover are out of phase, with deep convection peaking in the early morning throughout the equatorial Pacific. The diurnal cycle is strongest in the west Pacific and Indonesia, where deep convection is most intense. DCC top temperatures are at a minimum several hours before the maximum in DCC cover and out of phase with CAC top temperatures.

Two types of relationships between deep convection, SST, and surface wind convergence are suggested: 1) When a large area within a region is covered by SSTs greater than 28°C, deep convection is enhanced in areas where SST exceeds 28°C in the absence of strong surface divergence. Strong monthly mean surface convergence does not enhance deep convection in this case. 2) When the warmest SSTs in a region are less than about 28°C, deep convection is significantly enhanced by strong surface wind convergence near the local maximum in SST (26°–28°). An analysis of a slightly different version of the ISCCP data for the period July 1983–July 1985 suggests that the first type of relationship is the typical situation in the west Pacific, while the second relationship is most obvious in non-El Niño northern winters in the east Pacific. DCC top height generally increases as SST increases, but the visible reflectance of DCC does not vary strongly with SST.

1. Introduction

The global atmospheric response to heat sources in the tropics is among the most important questions about the general circulation. Deep convection is the primary mechanism for this response because it is the most effective means of transporting heat from the planetary boundary layer to the free troposphere (Riehl and Malkus 1958). In estimates of climate sensitivity to external forcing, cloud feedbacks are considered to be one of the greatest sources of uncertainty (Hansen et al. 1984; Schlesinger and Mitchell 1987; Wetherald and Manabe 1988). Convection, which is the most important process for transporting moisture from the lower to upper troposphere in the tropics, plays key roles in the temperature lapse rate feedback, water va-

por feedback, and radiative feedbacks associated with changes in large-scale clouds (Del Genio and Yao 1988).

The equatorial Pacific is also the seat of important interactions between the atmosphere and ocean that produce phenomena such as the El Niño/Southern Oscillation (ENSO) and monsoons. In the equatorial west Pacific, the warmest area in the tropical oceans, deep convection occurs as the 'root' of both the Hadley and Walker circulations, associated with dramatic latitudinal and longitudinal variations of cloud cover, precipitation, and SST. Changes in deep convection are believed to affect the global circulation (Simmons 1982).

Two approaches have previously been used to study variations of deep convection. Some investigators have analyzed precipitation data as a proxy for deep convection (Gray and Jacobson 1977); however, the low spatial density of observation sites, especially over

Corresponding author address: Ms. Rong Fu, NASA/GSFC, Institute for Space Studies, 2880 Broadway, New York, NY 10025.

oceans, makes it difficult to observe this phenomenon over a complete range of scales. Although total precipitation represents an integrated measure of the latent heating effect of convective complexes, the relation to cloud cover and consequent radiative heating of the surface and cooling of the atmosphere is not generally known.

Other investigators (Webster and Stephens 1980; Liebmann and Hartmann 1982; Murakami 1983; Hartmann et al. 1984; Ardanuy and Kyle 1986; Nitta 1986) have used various outgoing longwave radiation (OLR) datasets to study variations of tropical convection. These studies suffer from two limitations. First, for OLR measurements actually taken by a broadband radiometer (e.g., from Nimbus-7), the sensitivity to cloud variations, and the ability to discriminate between different high cloud types is reduced by the predominance of lower (colder) atmospheric emission over higher (warmer) surface emission when observing the whole thermal wavelength range. Moderately thick cirrus clouds may appear similar to thicker anvil clouds or even convective towers (especially given the lower spatial resolution of these broadband scanning radiometers). Thus, OLR contrasts between the east and west Pacific and between the tropics and subtropics will also depend on the distribution of water vapor and thinner high-level clouds as well as deep convection. Another commonly used OLR dataset is constructed from narrowband (wavelength $\approx 11 \mu\text{m}$) measurements by use of a linear regression relation (e.g., Liebmann and Hartmann 1982). While this approach may capture a proper global or regional mean value of the OLR, it may not represent the spatial and temporal variations of actual OLR correctly because the effects of changing water vapor are underestimated and changing low-level clouds are overestimated. On the other hand, these data may have higher sensitivity to cloud variations, since surface emission is more important at $11 \mu\text{m}$. Most analyses have used spatially averaged data, however, that reduce temperature contrast and hence sensitivity to changes of clouds.

A second limitation of both types of OLR studies is that they use constant OLR thresholds to discriminate between 'high' clouds and all other clouds or clear conditions. This simplistic approach mixes together at least two distinct types of cloud behavior, as we will show, and cannot account for variations of the high level cloud attributes with location and season. For some applications this may not be a severe limitation, since thin high clouds (tropical cirrus canopies) are usually associated with thick high clouds (mesoscale convective cloud clusters) (cf., Zipser 1977). However, the spatial scale of the mesoscale clusters is smaller than that resolved by most OLR studies, and this may be important in certain air-sea interaction problems (Zebiak 1990). Furthermore, the long lifetime of cirrus clouds compared to the deep convection that generates them

makes it difficult to deduce the diurnal cycle of convection with a single threshold.

The approach adopted here attempts to identify distinct subgroups of high-level cloudiness and to account for systematic variations in their properties. To this end, we employ both narrowband visible and infrared imagery from operational weather satellites to enhance sensitivity and to discriminate between thin and thick high level clouds. Visible radiances from satellites have been used in several previous studies of convective cloudiness (Minnis and Harrison 1984; Minnis et al. 1987; Rossow et al. 1990)¹. The additional visible channel makes a better isolation of convective towers from other high clouds possible (Del Genio and Yao 1987). Our purpose is to isolate and study deep convection as the initiator of a whole complex of phenomena that lead to atmospheric and surface heating/cooling. We use a statistical approach to derive identification criteria from the frequency distributions of the basic radiances (represented as visible reflectance and brightness temperature) in the ISCCP B3 data (Rossow et al. 1987). The B3 data, a primary data product of ISCCP, are a reduced-resolution, calibrated and normalized, infrared- and visible-radiance dataset (Schiffer and Rossow 1985).

In this paper, we describe a combined visible-infrared (VS-IR) method for detecting DCC and we use this method to adjust an equivalent IR-only method (section 2) for study of diurnal variations. We examine the characteristic features and the spatial distribution of deep convection, the diurnal cycle of deep convection, and the relation of deep convection to SST and surface wind divergence in the equatorial Pacific in sections 3, 4 and 5, respectively. Our discussion and summary are in sections 6 and 7.

2. Data and method

a. Data

We use the ISCCP B3 radiance data from the GMS-2 (Geostationary Meteorological Satellite of the Japan Meteorological Agency), stationed over 0° latitude and 140°E longitude, and from the GOES-6 (west) (Geostationary Operational Environmental Satellite of NOAA), stationed over 0° and 135°W . These radiances have been normalized to a specific radiometric standard by comparison to the NOAA-7 AVHRR (Advanced Very High Resolution Radiometer) and removal of any trends in AVHRR calibration (Rossow et al. 1987; Brest and Rossow 1990)².

¹ Stowe et al. (1988) use ultraviolet radiances in a similar fashion.

² Later comparisons of AVHRR and aircraft measurements suggest that the ISCCP B3 data we used underestimate reflectance systematically by 20% (Whitlock et al. 1990).

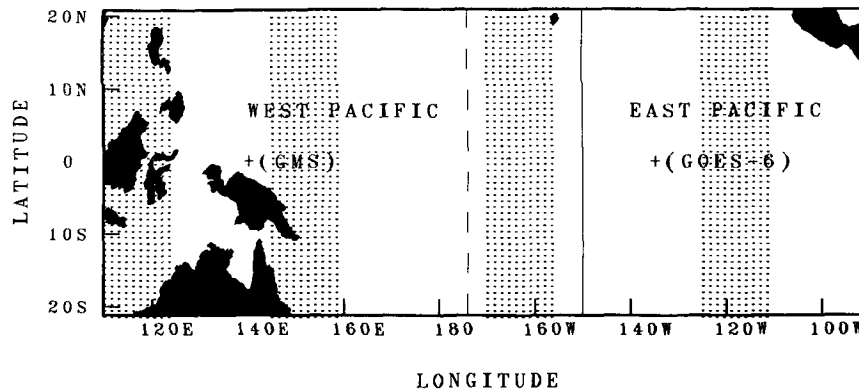


FIG. 1. The domain studied in this paper. The regions west and east of 175°W (dashed line) are covered by the GMS-2 and GOES-6 satellites, respectively. West Pacific and east Pacific are separated by the solid line. The longitudinal zones for which diurnal variations are analyzed are marked by dots.

The radiance data from these two satellites have a narrow-band visible channel (VS, $0.55\text{--}0.75\ \mu\text{m}$) and an infrared channel (IR, $10.5\text{--}12.5\ \mu\text{m}$) in common. The radiances are converted to reflectances (radiance scaled by the instrument solar constant and divided by cosine of the solar zenith angle) and brightness temperatures. The precision of the reflectances and temperatures are approximately $0.01\text{--}0.02$ and $0.5\text{--}1.0\ \text{K}$, respectively (Rossow et al. 1987). The original images (IR pixel resolutions of $5\ \text{km}$ and $8\ \text{km}$ at nadir³ for GMS-2 and GOES-6, respectively) have been sampled systematically to $25\text{--}30\ \text{km}$ spacing. There are eight images per day (UTC 0, 3, 6, 9, 12, 15, 18, 21). VS channel data exist for five daytime images; IR channel data are obtained for all images. The navigation information that determines the Earth location of each satellite image pixel, the observation geometry, and surface type information (land/water/coast) are also available in the ISCCP B3 dataset. We analyze data for July 1983 and January 1984; these months represent different phases of both the seasonal and El Niño cycles.

We also employ the Climate Analysis Center global SST data (Reynolds 1983) and the Florida State University (FSU) surface wind data (Goldenberg and O'Brien 1981) to investigate the relationship between deep convection, surface wind convergence, and SST in the equatorial Pacific Ocean. The monthly Climate Analysis Center SST data are derived from combined ground-based and satellite measurements with spatial resolution $2^{\circ} \times 2^{\circ}$ and reported accuracy of 1°C . The FSU monthly mean surface winds are based on ship measurements collected at a resolution $2^{\circ} \times 10^{\circ}$ but interpolated to a $2^{\circ} \times 2^{\circ}$ grid.

The most uncertain of these data are the wind data.

First, the surface wind data may not adequately represent the wind field over the lower troposphere. GATE data, for example, show that the divergence can change sign $100\text{--}200\ \text{mb}$ above the surface in the tropical Atlantic (Thompson et al. 1979). Gutzler and Wood (1990) find that the divergent component of the surface wind in the FSU data is not strongly correlated with the NMC 850 mb wind analysis over the tropical Pacific. This may, in part, be an indication of uncertainties in the analyzed winds that depend on uncertain GCM parameterizations. The tropical fields in the NMC and ECMWF analyses, for example, disagree in their details (Lambert 1988). Second, the temporal and spatial resolutions of the data are not sufficient to address fundamental questions about convection-dynamics relationships. The time scale of deep convection-convergence interactions is less than or comparable to the dynamic time scale, about one day. The FSU data give only the monthly mean wind and therefore average over many perturbations. The spatial resolution of the wind data is actually $2^{\circ} \times 10^{\circ}$, which may be too coarse to resolve the important spatial scales for deep convection-convergence interactions. Finally, the sparseness of observations causes large uncertainties in the wind data. However, the main features of the wind and divergence fields derived from the FSU wind data, e.g., the positions of the ITCZ (Intertropical Convergence Zone) and SPCZ (South Pacific Convergence Zone), and the magnitudes and locations of easterlies and westerlies, seem qualitatively realistic. Because of the limitations of the wind data, we view the convection-convergence comparison presented here as an experimental one which will eventually be superseded when more accurate tropical wind measurements become available.

Since our focus in this paper is on the equatorial Pacific, we restrict our study to the longitudes $124^{\circ}\text{E}\text{--}90^{\circ}\text{W}$ (Fig. 1). The latitude range $21^{\circ}\text{S}\text{--}21^{\circ}\text{N}$ is se-

³ Visible channel data are averaged to match the lower IR channel resolutions before sampling.

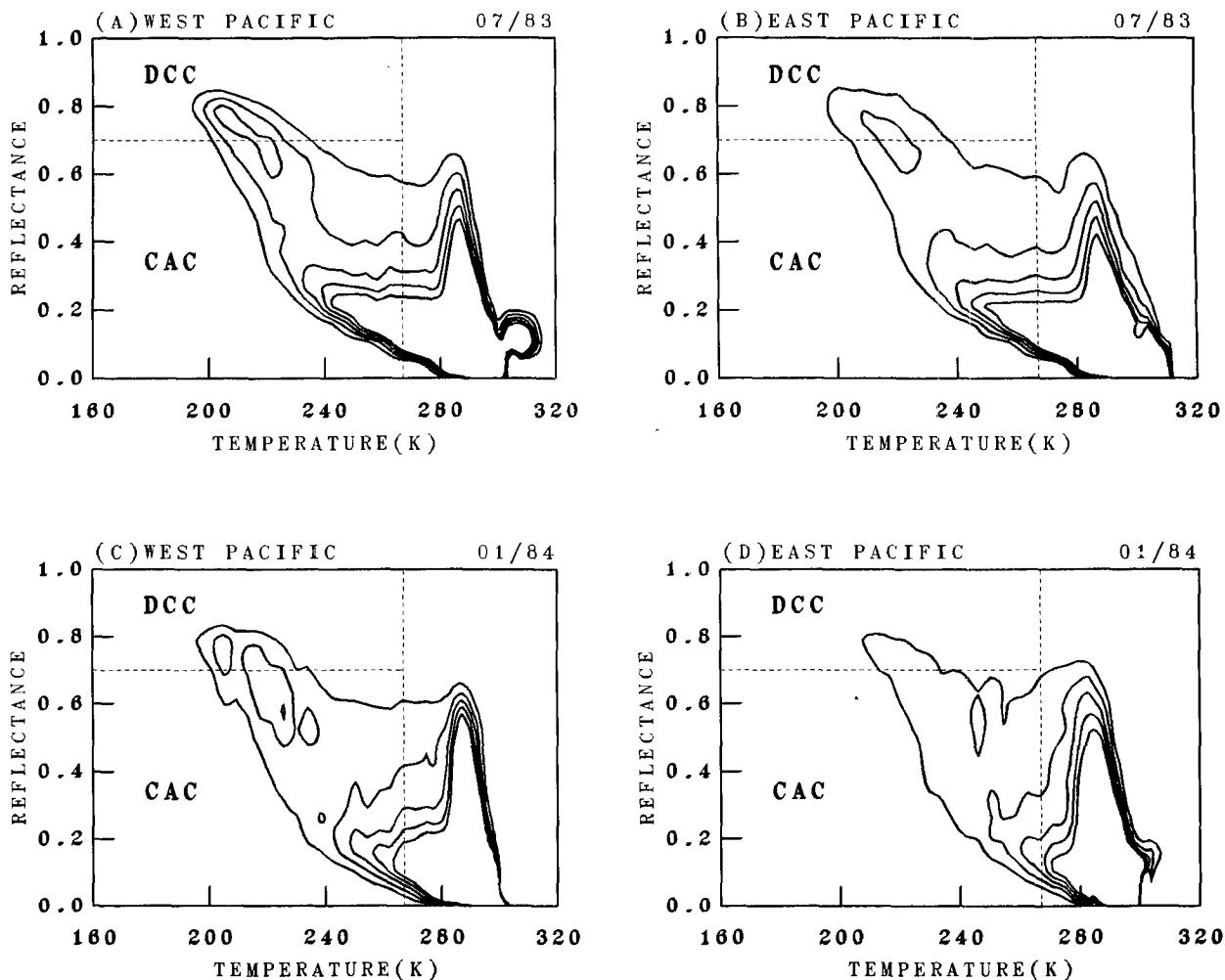


FIG. 2. Two-dimensional histograms showing the monthly mean frequency of occurrence of VS radiances expressed as reflectance (ordinate) and IR radiances expressed as brightness temperature (abscissa). Contours show equal increments in frequency; highest values in interior. (a) west Pacific, July 1983; (b) east Pacific, July 1983; (c) west Pacific, January 1984; (d) east Pacific, January 1984. The "DCC" and "CAC" domains are indicated in the figures.

lected to include most of the active area of the ITCZ and SPCZ.

b. Method

1) METHOD 1 (COMBINED VS-IR)

A key observation is that *at least* two distinct high level cloud types are found in the tropics. They are revealed by a difference in the correlated values of the visible and infrared radiances associated with them as illustrated in Fig. 2, which shows the normalized frequency histograms of all the pixels collected over one month⁴ for different parts of the domain at local noon

⁴ The histogram is the monthly mean number of pixels as a function of reflectance and temperature normalized by the number of total pixels in the corresponding part of the spatial domain.

as functions of VS radiance expressed as reflectance and IR brightness temperature. This method of displaying the data has been shown to be quite useful for delineating different cloud types and climatic regimes (Sèze and Rossow 1990). The type that we call DCC is associated with a distinct 'cluster' at reflectances about 0.6–0.8 and temperatures colder than about 240 K. The second type, which we call CAC, is associated with a more diffuse cluster that is darker and warmer than that of DCC⁵. Therefore we use a reflectance and temperature threshold method to distinguish DCC and CAC pixels from other pixels.

Although the thresholds used to identify DCC and CAC are somewhat arbitrary, the key to our results is

⁵ The histograms also suggest the presence of low-level clouds in the elongation along the VS axis at high IR temperatures.

the identification of stable subpopulations of high-level cloudiness. An example of spurious changes associated with changing attributes of the subpopulation is provided by the exaggerated apparent decrease in DCC in the eastern Pacific during January 1984, measured by a fixed IR-only threshold, part of which is caused by a systematic increase of cloud top temperature (Fig. 2d). The key to the proper identification of these clouds is the use of VS radiances that allow for a more flexible IR criterion than required to isolate DCC in the IR data only (see Section 2.2.2).

Since the distributions in Fig. 2 are continuous in the reflectance-brightness temperature domain, it is not possible to select "ideal" thresholds which admit all DCC and CAC while filtering out all other cloud types. Previous ground-based and satellite studies (Ogura and Cho 1973; Johnson 1980; Nitta 1986; Del Genio and Yao 1987) suggest a bimodal distribution of cloud top heights over the tropical oceans with a minimum near 500 mb. We therefore take 267 K, the climatological 500 mb temperature at 0°–20°N latitude (Crutcher and Meserve 1970), as our IR threshold to separate high-level from low-level cloudiness. This threshold may exclude some very thin cirrus, which transmit sufficient IR radiance from below to appear warmer than 267 K.

To select an optimum VS reflectance for separation of DCC and CAC, we tested 0.6, 0.65, 0.7, 0.75 and 0.80 as VS thresholds. The cloud top temperature distribution for each reflectance interval between 0.6 and 1.0 was examined. Figure 3a illustrates that, for reflectances higher than 0.7, the peak of the distribution is colder than 220 K, i.e., higher than the 200 mb level. Fewer than 17% of the clouds in this category have tops below the 300 mb (241 K) level and fewer than 6% below the 500 mb (267 K) level (Fig. 3b). For reflectances in the 0.6–0.7 range (Figs. 3c, 3d), the peak of the cloud top distribution is approximately or below 200 mb, but a second peak below the 280 K level becomes evident. Thus, a minimum reflectance of 0.7 effectively excludes clouds whose vertical extent is less than about 500 mb. Liou's (1976) radiative calculations indicate that only cumulonimbus and nimbostratus have reflectances this high⁶. Since nimbostratus are usually associated with frontal systems in midlatitudes, we expect that, in the tropics, clouds with reflectances greater than this minimum value are cumulonimbus (i.e., DCC). Therefore, it is possible to separate DCC from their associated cirrus and mesoscale anvils whose cloud bases lie in midtroposphere (Zipser 1977).

We choose 0.7 and 267 K as conservative reflectance and temperature thresholds (i.e., a few of the less optically thick DCC may be excluded, but everything that satisfies both criteria is likely to be a DCC). The mean DCC amount over our entire domain is then 2.0%, which is consistent with prevailing ideas about the areal coverage of deep convection (Sarachik 1980). To remove biases caused by varying scattering geometry, we use this combined VS-IR threshold method only for local noon images. This causes only a slight overestimation of the average over the complete diurnal cycle (see Fig. 8 and discussion in Section 4). The CAC are defined as pixels with reflectance darker than 0.7 and temperature colder than 267 K. The DCC and CAC domains are illustrated in Fig. 2.

Figure 4a is a time vs. longitude composite image (Hovmöller diagram) illustrating the spatial and temporal variability of the clouds detected by our VS-IR threshold method. CAC are typically organized on the mesoscale and propagate westward across the Pacific. This is consistent with the behavior of mesoscale anvils during GATE (Zipser et al. 1980). These clouds cover about 21% of the domain. Embedded within them are much smaller areas of DCC (pixels which exceed both thresholds), which show some tendency to decrease over the lifetimes of individual clusters. All of these features are consistent with the observed behavior of tropical convection (Houze and Betts 1981) giving us confidence that the technique can successfully distinguish tropical DCC from thinner CAC and shallow cumulus. Sensitivity of the derived cloud amounts to the VS threshold is summarized in Table 1.

Diagnosis of DCC poleward of the latitudinal range of our domain is not feasible with this method because of horizontal gradients in air temperature at the same altitude and because of the prevalence of thick frontal nimbostratus, which have similar radiative signatures, in midlatitudes.

2) METHOD 2 (IR ONLY)

Method 1 is limited to daytime images because at night only the IR channel is available. This prevents us from examining the full range of diurnal variability with method 1. Although several methods have been developed to detect DCC from IR radiance data (Murakami 1983; Meisner and Arkin 1987; Adler and Negri 1988), we study diurnal variations of DCC and associated CAC with an IR-only method adjusted to agree with method 1 at local noon.

Since the DCC can be distinguished from other clouds in daytime by our combined VS-IR threshold method, the characteristic cloud top temperature of the DCC, obtained by method 1, is employed as a guide for choosing an appropriate IR threshold [see Minnis and Harrison (1984) for a slightly different approach to this problem]. The characteristic temperature of the

⁶ Our VS threshold for DCC should be $1.2 \times 0.7 = 0.84$ when the underestimation of reflectance in the data is taken into account. This value agrees with the reflectance of DCC (0.8–0.9) obtained from some theoretical studies (cf., Liou 1976; Stephens 1978).

VS THRESHOLD TEST

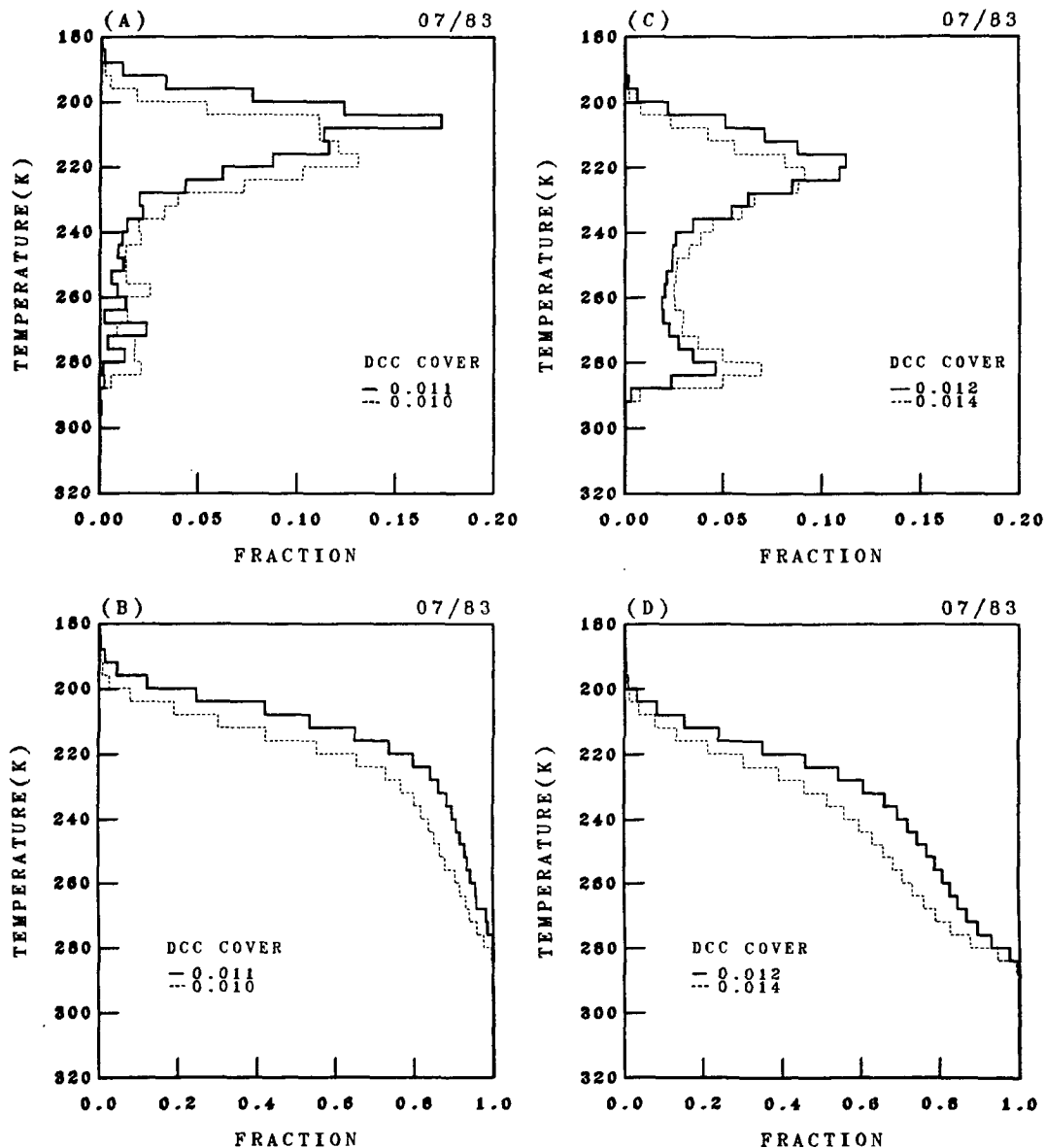


FIG. 3. Frequency histograms of the monthly distributions (a, c) and cumulative distributions (b, d) of brightness temperatures for pixels with reflectances in certain ranges in the west Pacific for July 1983. The reflectance ranges are (a, b) 0.75–1.00 (solid), 0.70–0.75 (dashed); (c, d) 0.65–0.70 (solid), 0.60–0.65 (dashed). The upper and lower DCC amounts are west Pacific means for the solid and dashed curves, respectively, in each figure.

DCC cluster suggested by Fig. 2 is about 220 K. We analyze distributions of reflectance for several cloud top temperature intervals for the equatorial west Pacific in July 1983 (Fig. 5). When the cloud top temperature is lower than 220 K, the peak of the reflectance distribution is greater than or comparable to 0.7. As cloud top temperatures become warmer than 220 K, the peak of the distribution shifts to lower reflectance and the fraction of low reflectivity clouds significantly increases.

This suggests 220 K as a first approximation for a cutoff to isolate DCC. The resulting cloud amount is comparable to that obtained by the VS-IR threshold method in January 1984, but much greater in July 1983 (Table 1). Taking 215 K as an IR threshold allows for better agreement with the VS-IR threshold method in July 1983 but worse in January 1984; however, the latter choice is more conservative. More than 70% of the clouds with IR temperature between 215 K and 220

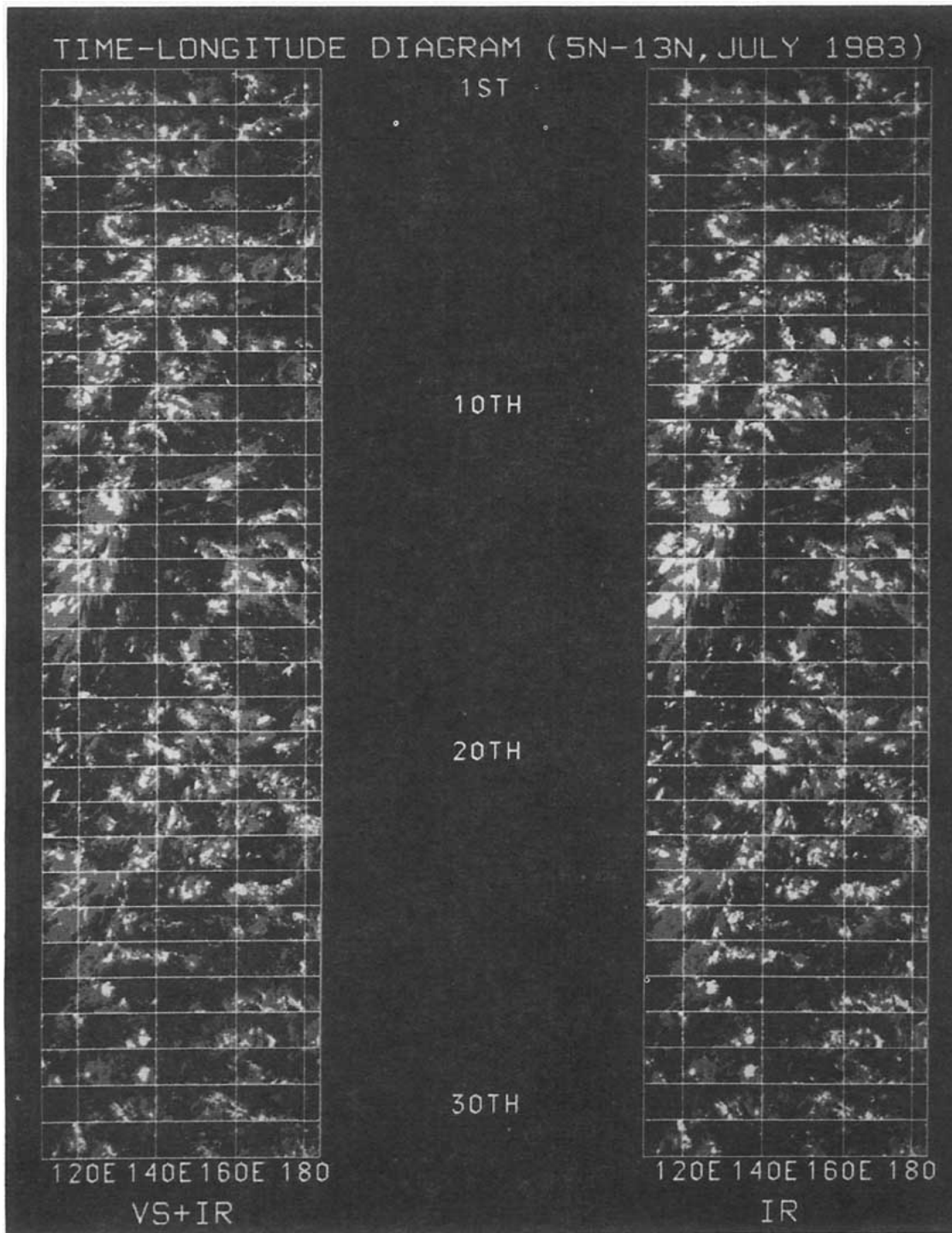


FIG. 4. Hovmöller diagram (time on vertical axis vs longitude on horizontal axis) of (a) VS-IR and (b) IR images for the region of 5°N–13°N, 110°E–175°W, July 1983. The white, gray and black represent deep convective cloud, cirrus/anvil cloud and absence of high cloud, respectively. (a) DCC is defined by using VS reflectance $R > 0.7$ and IR brightness temperature $T < 267$ K. Cirrus/anvil cloud is defined by $R < 0.7$ and $T < 267$ K. (b) DCC is defined by $T < 215$ K and cirrus/anvil cloud is defined by $215 \text{ K} < T < 267$ K.

TABLE 1. Summary of sensitivity of the derived cloud amounts to visible threshold (R = reflectance) and infrared threshold (T = brightness temperature). The numbers derived from the final choices of thresholds are underlined. OLR equivalents to various infrared thresholds are given in parentheses.

Threshold	DCC Amount (%)			
	July 1983		January 1984	
	W. Pacific	E. Pacific	W. Pacific	E. Pacific
Visible-Infrared				
$R > 0.80; T < 267$ K	0.3	0.2	0.9	0.1
$R > 0.75; T < 267$ K	1.1	0.7	1.8	0.5
$R > 0.70; T < 267$ K	<u>2.0</u>	<u>1.4</u>	<u>2.9</u>	<u>1.0</u>
$R > 0.65; T < 267$ K	3.1	2.2	4.1	1.8
$R > 0.60; T < 267$ K	4.3	3.0	5.3	2.5
Infrared-only (OLR)	W. Pacific	E. Pacific	W. Pacific	E. Pacific
$T < 210$ K (110 W/m ²)	1.2	0.8	1.5	0.3
$T < 215$ K (121 W/m ²)	<u>2.0</u>	<u>1.5</u>	<u>2.5</u>	<u>0.6</u>
$T < 220$ K (133 W/m ²)	3.0	2.1	3.4	1.0
$T < 241$ K (191 W/m ²)	8.2	5.5	8.8	4.2
$T < 255$ K (240 W/m ²)	12.4	8.4	13.1	6.9
$T < 267$ K (288 W/m ²)	17.3	11.4	18.3	10.1
Threshold	Cirrus/Anvil Cloud Amount (%)			
	July 1983		January 1984	
	W. Pacific	E. Pacific	W. Pacific	E. Pacific
Visible-Infrared				
$R < 0.80; T < 267$ K	17.0	11.2	17.3	10.0
$R < 0.75; T < 267$ K	16.2	10.7	16.5	9.6
$R < 0.70; T < 267$ K	<u>15.3</u>	<u>10.0</u>	<u>15.3</u>	<u>9.1</u>
$R < 0.65; T < 267$ K	14.2	9.2	14.2	8.3
$R < 0.60; T < 267$ K	13.1	8.4	13.0	7.6
Infrared-only	W. Pacific	E. Pacific	W. Pacific	E. Pacific
210 K < T < 267 K	16.1	10.6	16.7	9.8
215 K < T < 267 K	<u>15.3</u>	<u>9.9</u>	<u>15.8</u>	<u>9.5</u>
220 K < T < 267 K	14.4	9.3	14.9	9.1
241 K < T < 267 K	9.2	5.9	9.4	5.9
255 K < T < 267 K	4.9	3.0	5.1	3.2

K have VS reflectances less than 0.7; this decreases to 50% for clouds colder than 215 K (Fig. 5b,d). Also, Fig. 2 suggests that while complete separation of DCC from CAC in IR data is precluded by the continuous nature of the cloud-top temperature distribution, the local maximum in the histogram near 0.7 reflectivity is consistent with 215 K as a temperature threshold. For comparison, Table 1 also shows cloud amounts obtained for 241 K, the climatological temperature at 300 mb in the tropics (Crutcher and Meserve 1970), and for a 255 K threshold, which roughly corresponds to the 240 Wm⁻² OLR threshold often used to diagnose deep convection (cf., Murakami 1980; Lau and Chan 1985). These choices give much larger cloud cover dominated by contributions from CAC.

The longitude-time DCC and CAC distribution derived from method 2 (using the 215 K threshold) for images over the area of 5°N–13°N, 110°E–175°W for

July 1983 is presented in Fig. 4b. It appears very similar to that obtained by method 1 (Fig. 4a) in both coverage by DCC and in the morphology and propagation of individual features. Specifically, the IR-only CAC threshold in the images, defined as cloud top temperature between 267 K and 215 K, brings out the mesoscale cloud clusters that dominate the cloud field in this region, while the DCC threshold identifies convective cells embedded within the clusters. This convinces us that method 2 can replace method 1 *qualitatively* for the purposes of examining the diurnal cycle.

A quantitative comparison between method 1 and method 2 shows that about 50% of the clouds detected by method 2 are DCC as defined by our VS criterion for method 1. Conversely, about 50% of the DCC defined with the aid of VS data can be identified by the IR-only method. Since organized DCC systems are the dominant mode of tropical moist convection, it is likely

IR THRESHOLD TEST

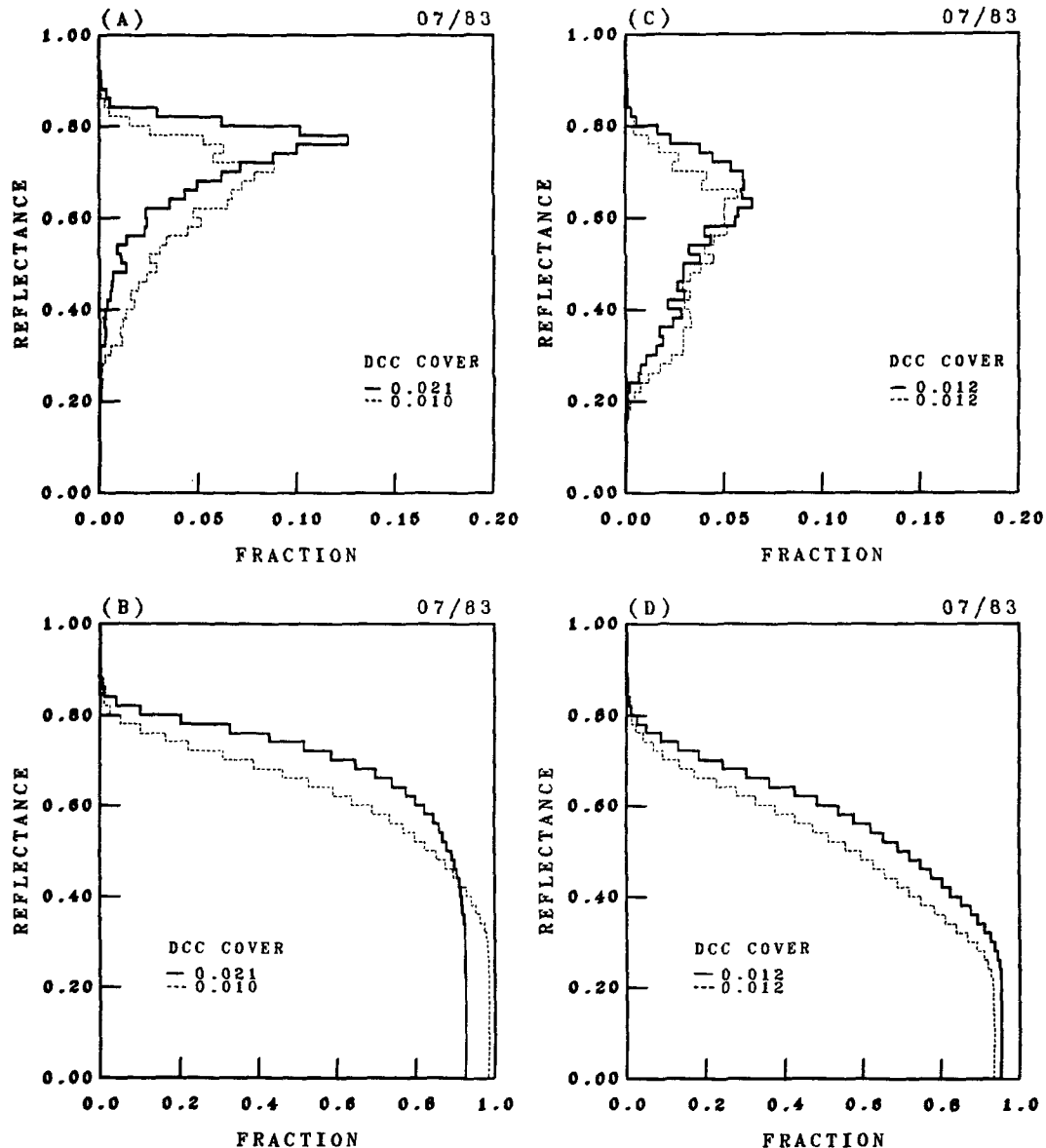


FIG. 5. Frequency histograms of the monthly distributions (a, c) and cumulative distributions (b, d) of reflectances for pixels with brightness temperatures in certain ranges in the west Pacific for July 1983. (a, b) <210 K (solid), 210 K–215 K (dashed). (c, d) 215 K–220 K (solid), 220 K–225 K (dashed). The upper and lower DCC amounts are west Pacific means for the solid and dashed curves, respectively, in each figure.

that most of the nonconvective clouds detected by method 2 are part of the cirrus/anvil canopy accompanying a DCC cluster (Fig. 4). Thus, we consider method 2 to be a satisfactory replacement for method 1. Steranka et al. (1984) investigated 23 tropical cyclones over the Atlantic Ocean and found that the mean cloud top altitude of deep convection near the center of tropical storms is near 12 km, while that of the dense

cloud canopy is about 9.7 km. This result is not surprising since deep convective updrafts can be quite vigorous and often overshoot their level of vanishing buoyancy. This result may explain our ability to distinguish DCC from their associated mesoscale anvils by choosing a sufficiently cold IR threshold. The IR-only method can be applied qualitatively to the narrow band OLR datasets by adopting the corresponding

OLR threshold (see Table 1). Table 1 also indicates the degree of sensitivity of our derived cloud amounts to the assumed IR threshold.

Sensitivity tests show that the VS-IR and IR-only methods give almost identical results except for the tropical east Pacific in January 1984. The reason for this discrepancy is that DCC tops in that area and month were about 8 K warmer (≈ 1 km lower) on average than those in the tropical west and central Pacific. Most deep convective clouds are thus excluded by using an IR brightness temperature threshold of 215 K. Method 2 underestimates the DCC amount in such cases (see Table 1). This exposes the major disadvantage of IR-only methods. The IR threshold should be tuned separately against the VS-IR threshold for the west Pacific and for the east Pacific. This suggests that while the VS channel provides somewhat redundant information, if we focus on any one region of active convection, it is more important for the diagnosis of convection in a variety of regions with different surface and atmospheric conditions.

3. The spatial distribution of deep convective clouds

Large-scale concentrations of DCC in the tropics define the rising branches of planetary scale circulations and the locations of peak diabatic heating in the tropical atmosphere. Heddinghaus and Krueger (1981) analyzed annual and interannual variations of OLR and suggested that the large year-to-year changes, especially in the equatorial Pacific, are probably associated with ENSO. Lau and Chan (1983a,b) used similar OLR data and showed the existence of two dominant modes of nonseasonal variations in the global tropics, which relate to the 2–3 month time scale and ENSO. Nitta (1986) found large seasonal variations of OLR, which are greatly affected by the summer and winter monsoons over Southeast Asia and Australia. Meehl (1987) systematically analyzed annual and interannual variability in the tropical Pacific and Indian oceans by using long-term OLR, cloud, precipitation, and sea level pressure data. The Southern Oscillation-type signals of the ocean–atmosphere system were detected and the extratropical variations associated with these signals were analyzed as well. We investigate the spatial distribution of DCC for July 1983 and January 1984 as defined by the combined VS-IR threshold method.

The monthly mean DCC fractions over the equatorial Pacific in July 1983 and January 1984 are shown in Figs. 6 and 7. Traditionally, regions of high DCC cover have been used to identify the ITCZ and SPCZ in satellite images because these latitudes are collocated with the climatological ITCZ and SPCZ. However, on the monthly time scale, as indicated in Figs. 6 and 7, the DCC pattern does not necessarily correspond with the surface wind convergence pattern, particularly in the longitudinal direction. In both months a well-de-

fined ITCZ (with DCC cover as high as 12%) existed in the west Pacific near 5°N latitude, extending eastward slightly beyond the dateline. In the east Pacific, the ITCZ was shifted northward to 10°–15°N latitude. The east Pacific ITCZ was broad and confined to regions near the Central American coast in July 1983, with little DCC in the central Pacific. In January 1984, this feature was narrower and extended further into the central Pacific, with less convection near the coast. These changing DCC patterns in the central and east Pacific are consistent with OLR differences between El Niño and climatology (cf., Heddinghaus and Krueger 1981). The SPCZ was located between 2°S and 8°S in July 1983, but shifted to 10°–20°S and intensified in January 1984. East of 140°W longitude, there was little DCC cover south of the equator in either month. The SPCZ behavior is consistent with the seasonal climatology of the SPCZ (Meehl 1987).

In July 1983, the location and shape of the ITCZ and SPCZ are fairly well defined by the 28°C SST contour, in agreement with the conclusion of Graham and Barnett (1987). January 1984 is quite different in two respects. First, we find large DCC cover in the east Pacific overlying water with SST between 25°C and 27°C. Second, within the region of warm SST in the west Pacific, strong deep convection is confined to a narrower latitudinal band than is the distribution of SST itself. Especially near the equator, there are extensive areas of warm water without strong divergence and with little deep convection.

The spatial distribution of DCC top temperature is illustrated in Fig. 2. In July 1983, the DCC clusters in the west Pacific and the east Pacific have very similar reflectance and temperature values. In January 1984, DCC properties in the west Pacific are similar to those in July 1983, but DCC in the east Pacific are more shallow (warmer cloud tops) and less frequent than in July 1983. The DCC in the west Pacific for both months and in the east Pacific in July 1983 peaked at approximately 204 K–212 K; DCC in the eastern Pacific in January 1984 peaked at 212 K–220 K, approximately 1 km more shallow than in July 1983 (if we assume a lapse rate close to dry adiabatic in the upper troposphere). These differences may be evidence of suppression of DCC by the downwelling branch of the Walker circulation during non-El Niño winters and relaxation of the Walker circulation during El Niño periods.

4. Diurnal variation

In the previous section, we used the monthly average DCC distribution at local noon as a representation of the monthly averaged daily mean distribution of DCC. This raises the question of whether diurnal variations of deep convection in different parts of the tropical Pacific bias our impression of the spatial DCC distribution derived from local noon data. The diurnal cycle

PACIFIC OCEAN(2X2)

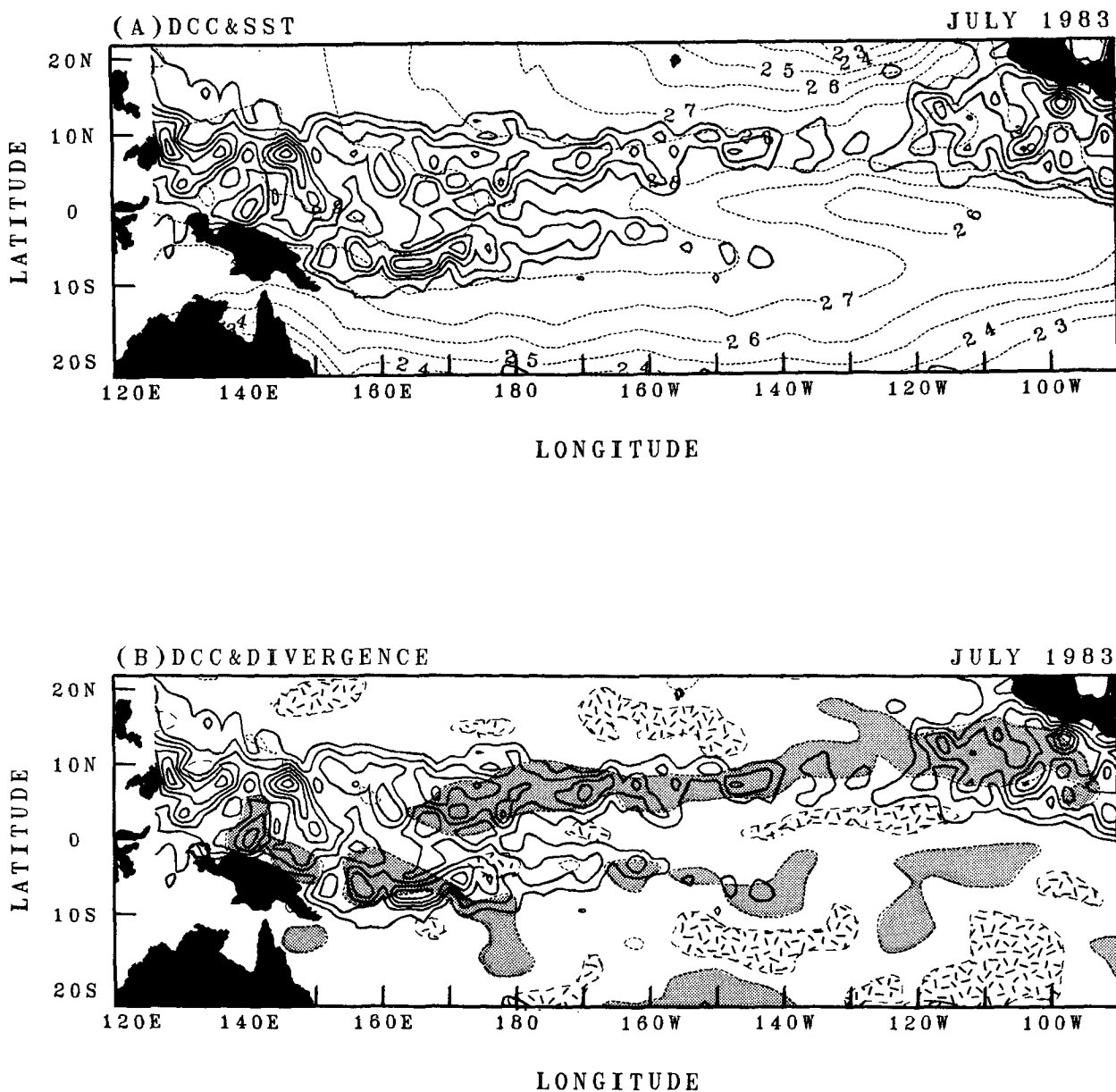


FIG. 6. (a) The spatial distribution of DCC obtained from the combined VS-IR method in July 1983. The solid contours (interval 0.02) represent the monthly DCC amount averaged over a $2^\circ \times 2^\circ$ grid box. The dashed contours represent monthly mean SST ($^\circ\text{C}$). (b) Surface wind convergence (shaded and hatched areas represent strong convergence and divergence, respectively, as defined in the text) and DCC cover as defined in (a).

of deep convection over the tropical oceans is also of interest itself as a possible means of diagnosing DCC forcing mechanisms, e.g., radiative-convective processes.

We use the IR-only threshold method to study the diurnal variations of DCC and CAC over the equatorial

Pacific Ocean. The advantage of our technique over those used in previous studies is that our IR-only method has been compared with the combined VS-IR threshold method and shown capable of discriminating between DCC and the thinner, lower CAC. We divide the equatorial Pacific into four subregions (Fig. 1) rep-

PACIFIC OCEAN(2X2)

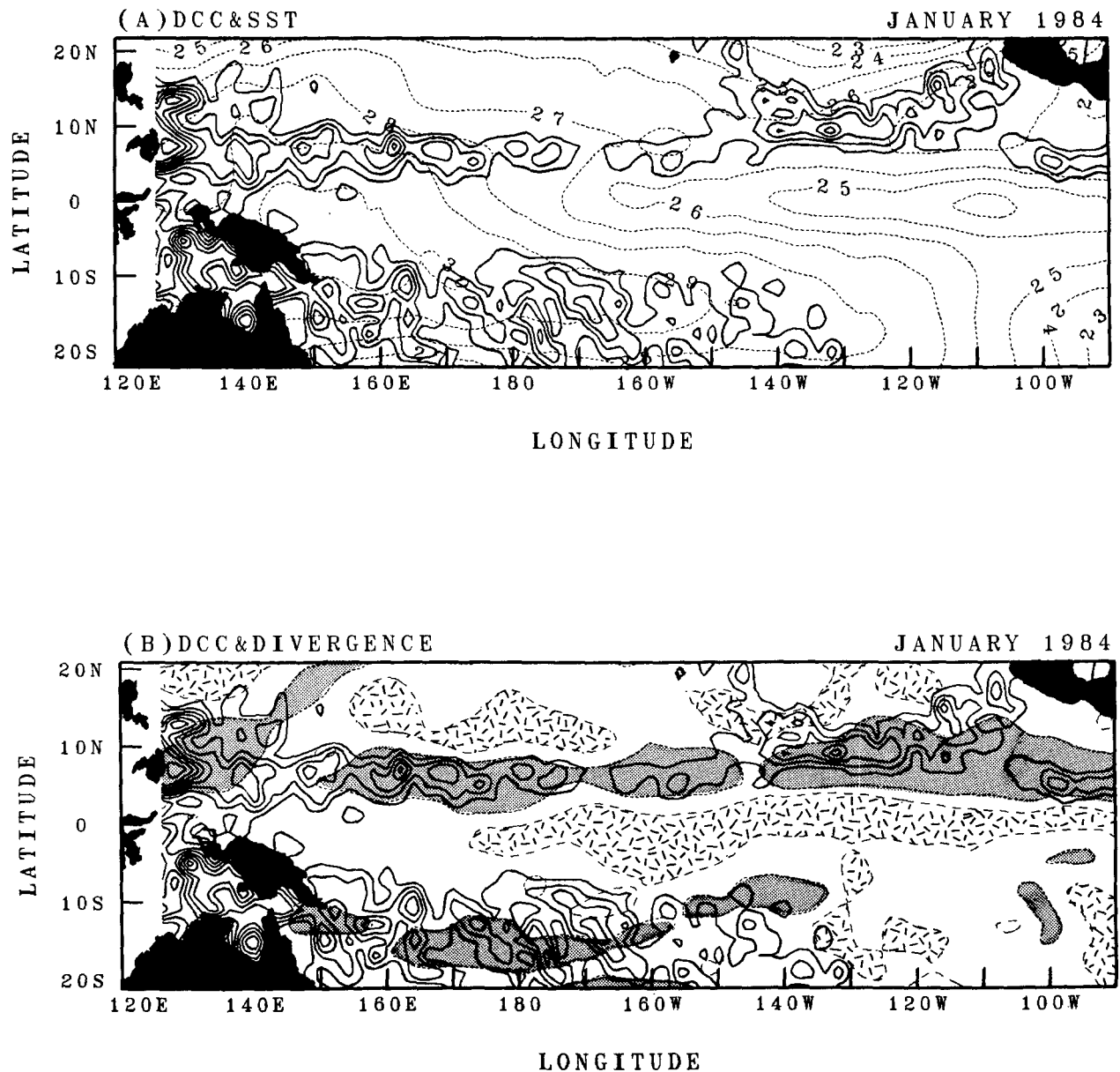


FIG. 7. As in Fig. 6 but for January 1984.

representative of Indonesia, the west Pacific, the central Pacific and the east Pacific, respectively.

Figure 8 shows the diurnal variations of DCC and CAC over ocean (all DCC and CAC over land pixels have been excluded from the analysis in this section) in the four subregions in July 1983. The diurnal cycles of DCC amount consistently peak in the morning and minimize in the afternoon in these four regions across

the entire equatorial Pacific. In the Indonesian area, the west Pacific, and the east Pacific, DCC amount reaches a maximum around 0700 local time (LT) and a minimum around 1900 LT. In the central Pacific, the peak was at approximately 0400 LT, 3 hours earlier than in the other regions. However, the real phase shift of DCC in the central Pacific might be somewhat smaller or larger than this because the time resolution

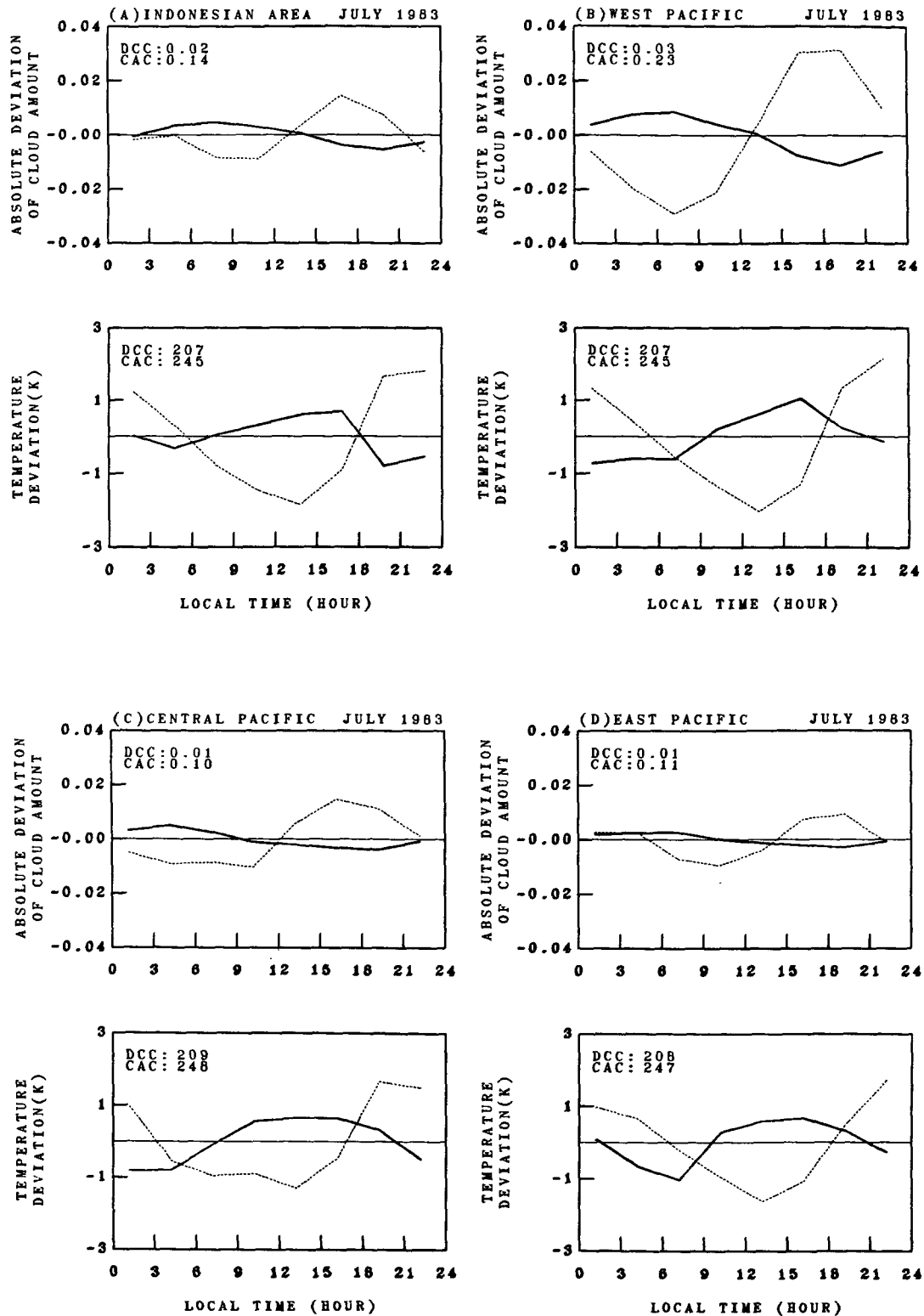


FIG. 8. The monthly mean diurnal cycles of DCC and CAC in July 1983 for (a) the Indonesian area, (b) the west Pacific, (c) the central Pacific, and (d) the east Pacific, as defined in Fig. 1. Upper: absolute deviation of cloud amount from daily mean. Lower: absolute deviation of cloud top temperature from daily mean. The solid curves represent DCC, and dashed curves represent CAC. The DCC and CAC numerical values are daily means for the solid and dashed curves, respectively, in each figure.

of the data is 3 hours. The absolute amplitude of the diurnal cycle varied from 0.3% to 1.0% in DCC amount, and the relative amplitude of the diurnal cycle was 20%–40% of the daily mean DCC amount. These results indicate that our estimate of the daily mean DCC amount is not significantly biased by using the value obtained at local noon. The noon value is a slight overestimate in the Indonesian area and the west Pacific and a slight underestimate in the central Pacific and the east Pacific (<10% in all cases).

The diurnal cycles of CAC amount were 135°–180° out of phase with those of the DCC. The absolute amplitudes were 1%–3% in CAC amount, larger than those of DCC, but the relative amplitudes were only about 15%, smaller than those of DCC. The phase difference cannot simply be explained as an artifact of dividing the results into two cloud types because the absolute amplitude of changes in CAC exceeds that for DCC. Zipser et al. (1980) hypothesized a time series of mass and precipitation fluxes associated with a typical mesoscale precipitation event in which the rainfall rate from the anvil reaches its maximum between the mature and dissipating stages, many hours after the peak in convective rain. The phase lag between DCC and CAC in our data is consistent with Zipser's hypothesis. In the east Pacific, a weak semidiurnal variation of CAC also appears. The absolute deviations of DCC and CAC are largest in the west Pacific, the most extensive DCC area.

DCC top temperatures are a minimum near or several hours before the time of maximum in DCC cover (Fig. 8); the same is true of CAC top temperatures. As with cloud cover, the amplitude of CAC temperature variations exceeds that for the DCC.

In January 1984, diurnal cycles of DCC and CAC were qualitatively similar to those of July 1983 in the Indonesian area and the west Pacific, although the diurnal amplitude in Indonesia was larger. This may reflect the influence of land on the diurnal cycle of DCC over ocean due to the closer proximity of the DCC zone to land (Borneo and New Guinea) in January 1984⁷. Although no DCC or CAC over land are included in the results, the diurnal variation of DCC over land could affect the diurnal variation of DCC over nearby ocean through a 'sea breeze' circulation. The diurnal cycle of DCC over land (not shown) is stronger and almost 180° out of phase with that over the ocean. In the afternoon, when DCC cover over land is a maximum, it may further suppress DCC over the nearby ocean, which is at its diurnal minimum, by stabilizing the atmosphere through enhanced subsidence. In the early morning, when DCC cover over land is a minimum, subsidence over land and rising motion over the ocean may produce a peak in the

oceanic diurnal cycle. The diurnal cycles of DCC in the central and east Pacific in January 1984 were not well defined. This may be due to the low frequency of occurrence of DCC in these regions during this month (Fig. 7), which is caused in part by the threshold used in the IR-only method (Fig. 2d).

Gray and Jacobson (1977) analyzed ground-based precipitation data from eight islands in the western tropical Pacific and found a consistent diurnal cycle with the maximum value in the morning and minimum value around early evening. They also pointed out that the more intense the deep convection is, the more evident is the diurnal cycle. They interpreted this diurnal variation to be caused by day versus night variations in tropospheric radiational cooling between the convective cloud and the surrounding cloud-free area. The diurnal phase of precipitation is the same as that of DCC in our results, implying that the diurnal variation of precipitation is dominated by DCC rather than CAC. GATE observations (Zipser et al. 1980; Houze and Betts 1981) indicate that at least 60% of the total precipitation is contributed by deep convection (our DCC) and 40% by the mesoscale anvils (our CAC). These results can be reconciled by noting that DCC produce more precipitation per unit area than CAC and that the nearly equal contribution to the total precipitation produced by the two cloud types is a result of the larger area covered by CAC relative to DCC.

Inferring precipitation from satellites is currently the only possible way to obtain information with satisfactory space/time sampling over oceans. Our results imply that using a single threshold value to relate IR radiances to precipitation, as is done in most studies (cf., Arkin and Ardanuy 1989), can produce misleading results by assigning equal significance to all locations with IR temperatures colder than the threshold value. If the two types of clouds contribute differently to the total precipitation, then separating them in the analysis, as we have done, seems necessary for a proper determination of precipitation variability. In particular, since the CAC are warmer than the DCC and cover a much larger area, they have a stronger influence on diurnal variations of OLR. Hartmann and Recker (1986) found a maximum of OLR in the morning and concluded that this variation is dominated by clouds near the 400 mb level; both of these results are consistent with the minimum of CAC amount that we find at this time of day. Contrary to their conclusion, however, this is not consistent with the surface precipitation measurements. Albright et al. (1985) also used a single threshold in their analysis, which was consistent with the behavior of OLR in the GATE region; but it is apparent in their results that the phase of the diurnal cycle varies with height in the Pacific. By using a single threshold (–36°C, which is equivalent to the 300 mb level, approximately), they convolve the behavior of the DCC and CAC: precipitation in the SPCZ inferred

⁷ This possibility was suggested by an anonymous reviewer.

from OLR peaks in the afternoon, while surface observations at Canton, Tarawa and French Polynesia show a maximum in the morning (Finkelstein 1964).

5. Relationships between deep convection, sea surface temperature, surface wind convergence and evaporation

An understanding of the relations between deep convection and large-scale variables is required to model the onset of deep convection and the interaction between convection and the large-scale circulation. Thermodynamically, deep convection exists only if two requirements are satisfied: conditional instability throughout the lower troposphere and a means for air parcels to rise to the level of free convection (LFC). Conditional instability depends only on the atmospheric lapse rate. The second condition is determined by the altitude of the LFC, which depends upon the humidity and temperature of the planetary boundary layer (PBL). It is also influenced by the depth of the PBL, which is controlled by turbulence and low-level wind convergence. In the PBL, temperature approximately follows SST and humidity is determined by evaporation, low-level moisture convergence, and deep convection. Moisture convergence $\nabla \cdot (q\mathbf{V})$ (where q and \mathbf{V} represent the specific humidity and wind velocity, respectively) is thought to be dominated by low-level wind convergence $q\nabla \cdot \mathbf{V}$ because small humidity gradients in the tropics (Oort 1983) limit the contribution of the horizontal advection term $\mathbf{V} \cdot \nabla q$. Above the PBL, the temperature profile is controlled by the large-scale circulation driven by convection and radiation.

Early observations (Bjerknes 1969; Rowntree 1972; Julian and Chervin 1978) suggested a linkage between SST anomalies and deep convection. It was originally assumed that local evaporation, which was thought to be controlled by SST, was the dominant moisture source for deep convection. However, recent estimates by Liu (1988) indicate that local evaporation variations depend not only on SST anomalies, but also on the variation of low-level wind, especially in regions of convergence. Cornejo-Garrido and Stone (1977) showed that convection is usually correlated with minimum evaporation. This implies that low-level convergence must supply most of the local moisture for convection. This conclusion was confirmed by Thompson et al.'s (1979) comprehensive study of easterly wave disturbances in the tropical eastern Atlantic during GATE. Khalsa (1983) examined correlations between SST, rainfall, low-level moisture convergence and evaporation for the central and east Pacific during the 1972–73 El Niño. Khalsa claimed that rainfall is more closely related to moisture convergence and attributed the good correlation (0.68) between SST and rainfall to a good correlation (0.86) between SST

and low-level convergence. Steiner (1987) found that in the tropical Pacific from 5°N–15°N and 0°–15°S winds blowing opposite to the normal easterly trade wind flow are more likely to be accompanied by strong convection.

Graham and Barnett (1987) studied long-term low-frequency variations of deep convection, SST and low-level convergence at 50 sites in the equatorial Indian, Pacific, and Atlantic oceans and suggested that there is a critical SST of about 27.5°C in the tropical oceans below which deep convection generally does not occur. In areas with SST > 27.5°C, convection becomes insensitive to SST variation and prefers regions with significant low-level convergence. Below 27.5°C, evaporation controls convection. Above 27.5°C, low-level wind convergence becomes more important. Model results support the idea of a critical SST for tropical Pacific convection (Neelin and Held 1987; Del Genio and Yao 1988; Lau and Shen 1988).

Figures 9 and 10 show the relationship of deep convection, as defined by our VS-IR technique, to monthly mean SST, surface wind divergence, and evaporation in the tropical west and east Pacific for July 1983 and January 1984. The boundary between these two regions is placed at 150°W (Fig. 1) because, as we will see, the behavior of deep convection and its relation to SST and convergence is different east and west of this longitude at times (e.g., January 1984) probably due to the difference in static stability in these two regions (Reed and Recker 1971; Garcia et al. 1986). We cannot measure evaporation directly. For this comparison we have made a crude estimate based on the observed SST and surface wind fields using a bulk aerodynamic formula $E = 0.22U\rho_a C_p C_D q^*$, where U denotes surface wind speed, ρ_a the density of air at the surface, C_p the specific heat at constant pressure, C_D a drag coefficient of 0.001 (Smith and Banke 1975) and q^* the saturation mixing ratio. The sea–air temperature difference is assumed to be 0.5°C (Hsiung 1986) and the surface relative humidity is taken to be 78% (Oort 1983), both typical values for the tropical oceans. The calculated evaporation shows a reasonable spatial structure with magnitudes consistent with Liu's (1988) inferences near the equator. Evaporation estimated in this way induces some correlation between evaporation and SST or surface wind.

Since the variables we seek to relate DCC are significantly correlated with each other, it is difficult to isolate the effect of any one variable. For a clearer presentation of the enhancement or suppression of DCC, we define a DCC index as follows. Let N_{ci} be the number of gridboxes with "extensive" deep convection in regime i defined by combinations of SST, wind divergence, and evaporation (Figs. 9a and 10a) and let N_c be the total number of gridboxes with extensive convection summed over all regimes. We define extensive deep convection as a monthly mean DCC amount

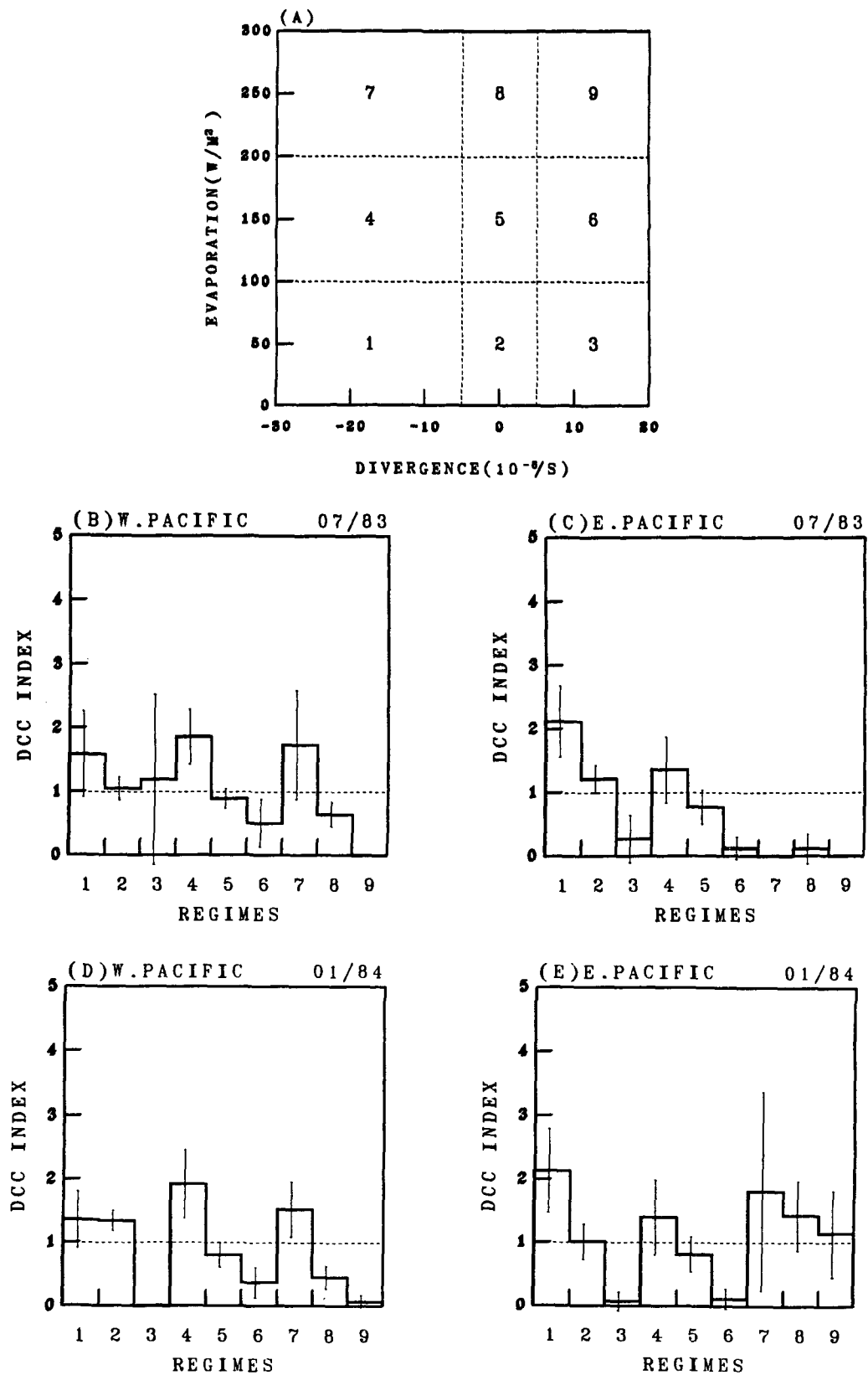


FIG. 9. (a) Definition of evaporation-divergence regimes. The numbers in the boxes are those indicated along the abscissa in Figs. 9b-e. (b) Histograms of the DCC index defined in the text as a function of regime for the west Pacific in July 1983. The error bars for the DCC index values are 95% confidence intervals estimated by assuming a binomial distribution of extensive DCC grid boxes in the 9 regimes (Scheaffer and McClave 1982). (c) As in (b) but for the east Pacific. (d) As in (b) but for January 1984. (e) As in (c) but for January 1984.

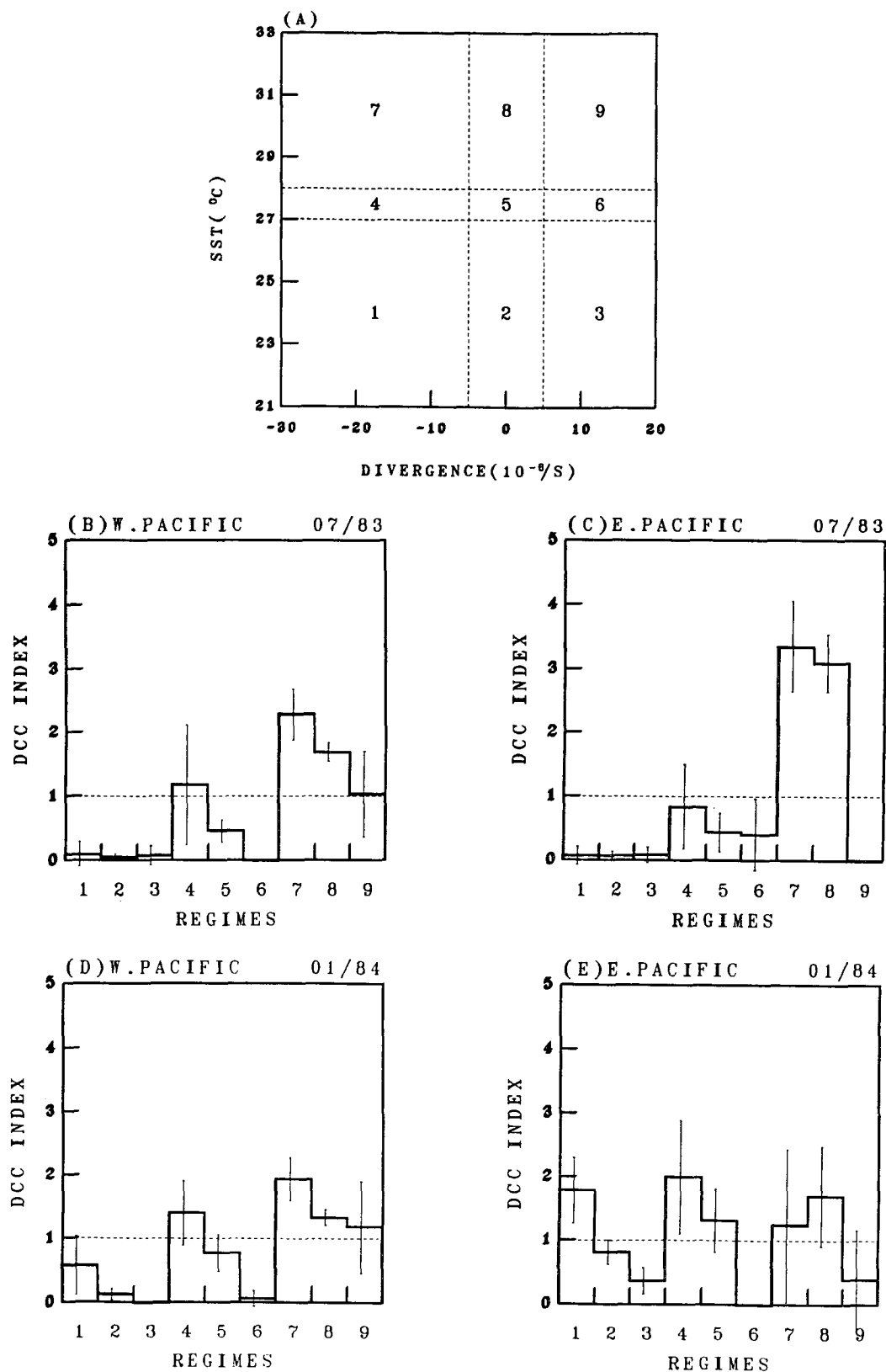


FIG. 10. As in Fig. 9, but for SST-divergence regimes.

greater than 2%, the mean for the whole tropical Pacific. Let N_i and N represent the total number of gridboxes in regime i and in the total domain, respectively. Then we calculate the DCC index as $(N_{ci}/N_c)/(N_i/N)$. When DCC are enhanced, i.e., the fraction of grid boxes with extensive DCC which occur in a regime is greater than the fractional area of the regime, the DCC index is greater than 1. When DCC are suppressed, the DCC index is less than 1.

Figure 9 shows the DCC index as a function of local evaporation and surface wind convergence for the tropical west Pacific and east Pacific. The evaporation-divergence domain is divided into 9 regimes (Fig. 9a). Evaporation is arbitrarily classified as weak, medium or strong based on dividing the range of surface latent heat flux estimates in our domain ($0\text{--}300\text{ W m}^{-2}$) into three equal intervals. The wind divergence axis is divided into strong convergence, weak convergence/divergence and strong divergence categories. The middle category includes all points whose divergence is less in magnitude than the maximum longitudinal mean divergence for the $21^\circ\text{N}\text{--}21^\circ\text{S}$ domain ($5 \times 10^{-6}\text{ s}^{-1}$). Figures 9b–9e show no consistent relationship between extensive DCC and evaporation: DCC indexes are not consistently higher or lower in a particular evaporation category which is consistent with Khalsa's (1983) finding of a low correlation (0.26) between evaporation and rainfall.

Based on previous work (Cornejo-Garrido and Stone 1977; Thompson et al. 1979; Khalsa 1983; Graham and Barnett 1987), we expect to see a good correlation between deep convection and surface wind convergence. The relatively high amount of extensive deep convection in areas of strong surface convergence (regime 1 in the east Pacific and regime 4 in the west Pacific for both months) seems to bear this out. However, in some strong convergence regimes, for example, regime 1 in the west Pacific, strong convergence does not always enhance DCC by a statistically significant amount. In fact, even if deep convection is well correlated with low-level convergence on short time scales, it may not correlate as well with monthly mean convergence. A few transient episodes of convergence (e.g., due to passing easterly waves) in a region that is otherwise divergent, may be sufficient to produce a substantial monthly mean DCC amount. Thus, even though the surface wind dataset we used is considered one of the best surface wind datasets available (Goldenberg and O'Brien 1981), neither its accuracy nor temporal resolution may be adequate to study the convection–convergence relationship.

The relationship of deep convection, SST, and surface divergence is presented in Fig. 10. We define cool and warm SST categories as SST lower than 27°C and higher than 28°C , respectively (Fig. 10a), after Graham and Barnett (1987). The SST range $27^\circ\text{C}\text{--}28^\circ\text{C}$, which is comparable to the uncertainty in the SST data, is

defined as a transition category. In July 1983 (Figs. 10b and 10c), when the longitudinal gradients of SST are small and warm water ($\text{SST} > 28^\circ\text{C}$) extends across the entire Pacific near the equator (Fig. 6a), the correlation of deep convection with SST and convergence is qualitatively the same in the west and east Pacific. The high DCC indices in regimes 7 and 8 in both regions show that DCC are greatly enhanced in the areas of $\text{SST} > 28^\circ\text{C}$ as long as strong divergence is not present. Actually, about 90% of the extensive DCC gridboxes occurs in these areas. The near-zero DCC indexes in cold SST areas (regimes 1, 2 and 3) and lower DCC indexes in the transition SST area indicate that DCC are significantly suppressed in areas of $\text{SST} < 28^\circ\text{C}$, even when surface convergence is strong.

In January 1984 (Figs. 10d and 10e), the relation of extensive deep convection to SST and convergence remains the same as that in July 1983 in the west Pacific (hereafter we call this the west Pacific type of relation). However, in the east Pacific, where there are few locations with SST greater than 28°C , considerable deep convection still occurs, more than 60% of it in areas of cool SST. The DCC index is significantly higher than 1 in regimes 1 and 4, suggesting that DCC were enhanced in areas of strong surface wind convergence and $\text{SST} < 28^\circ\text{C}$. Large uncertainties in the warm SST areas are caused by the small number of samples there; thus, it is hard to tell how extensive DCC are related to surface wind in this situation.

These results suggest that there are at least two types of relation between deep convection, SST and surface wind convergence. One is the west Pacific type. The other is the east Pacific type, which is observed in the east Pacific only when SST is not abnormally warm. We have performed a similar analysis for the first two years of ISCCP C1 data (July 1983–July 1985) by using an analogous threshold method. In the ISCCP C1 dataset the visible optical thickness of clouds, derived from B3 radiances using a radiative transfer model, and cloud top pressure can be used to define DCC (Rossow et al. 1988). The resulting inferences about the DCC pattern and the DCC–SST–surface wind convergence relationship from the C1 data agree very well with those from the B3 data shown in this paper for July 1983 and January 1984. This gives us confidence in the consistency of the two analyses and also illustrates the insensitivity of our results to the exact thresholds used to detect DCC.

The west Pacific type of relation (characterized by DCC index higher than 1 in regimes 7 and 8) occurs in 16 months out of the 20 months we analyzed in the west Pacific (months that contain less than 20 days of local noon data are excluded in the analysis). In the other four months, a hybrid relationship with characteristics of both the west Pacific type and the east Pacific type exists in the west Pacific. This suggests that the west Pacific type of relation is the dominant be-

havior in this region and does not vary qualitatively with season or during an ENSO event. In the east Pacific, when SST is mostly colder than 28°C (8 non-summer months out of 20 months), the DCC index is greater than 1 in regime 1 and 4, which defines the east Pacific type of relation. When there is a considerable area with $\text{SST} > 28^{\circ}\text{C}$ (9 out of 20 months), the DCC index is greater than 1 in regimes 1 and/or 4, as well as in 7 and/or 8. This behavior is a hybrid of the west Pacific type and the east Pacific type of relationship. When the area of SST warmer than 28°C extends more or less across the whole equatorial Pacific, such as in July 1983 (a decaying El Niño), March 1984 and April 1984, the DCC index exhibits the west Pacific type of relationship.

We have also considered the possible influence of SST gradients on the DCC-SST-surface wind convergence relationship in the east Pacific (cf., Lindzen and Nigam 1987; Gutzler and Wood 1990). For example, we have compared two pairs of months with similar total areas of $\text{SST} > 28^{\circ}\text{C}$ but with different meridional SST gradients in the east Pacific (March and April 1985 vs. December 1983 and November 1984). The relationships are not qualitatively different between these two cases. On the other hand, meridional gradients of SST are similar for March and April in 1984 and for the same months in 1985. However, the west Pacific type of relationship occurs in March and April 1984, while the east Pacific type of relation occurs in March and April 1985. Thus the relationship does not appear to explicitly depend on the instantaneous SST gradient. This, however, does not mean that the effect of SST gradient is not important. In fact, the major effects of SST gradient have been included in the surface wind divergence field and the surface latent heat flux field. Thus the only effect of SST gradients left out of our analysis is the sensible heat flux, which is believed to be one order of magnitude smaller than the latent heat flux. The role of surface wind convergence, and thus indirectly the SST gradient, defines the east Pacific type of relationship.

The relationship of DCC-SST-surface wind convergence obtained in our analysis appears different from Graham and Barnett's (1987) finding. The relationships we find suggest that DCC is not significantly enhanced in areas of strong surface convergence when $\text{SST} > 28^{\circ}\text{C}$. There are two possible explanations for this difference. First, while their analysis covers a much longer time period, the spatial sampling is very sparse. Both their analysis and ours do not have enough examples of strong surface wind divergence and $\text{SST} > 27.5^{\circ}\text{C}$. Second, their data sample only includes a range of surface wind divergence magnitudes less than $4 \times 10^{-6} \text{ s}^{-1}$, which is within our "weak" (near-zero) convergence category. To reduce the uncertainty in the divergence below $4 \times 10^{-6} \text{ s}^{-1}$ requires accuracies of wind measurements better than 0.5 m s^{-1} . Halpern

(1988) has pointed out that the number of random wind observations required per month for a 0.5 m s^{-1} accuracy in the mean is about 35 at a site in the 95° to 152°W region, which is much higher than typical for the equatorial Pacific. Thus the appearance of the lower OLR samples in the $0-4 \times 10^{-6} \text{ s}^{-1}$ convergence range in Graham and Barnett's Fig. 6 may not reliably indicate that convection occurs only in surface wind convergence areas. Graham and Barnett also did not include any areas of the east Pacific with $\text{SST} = 25^{\circ}\text{C}-27^{\circ}\text{C}$ in which we found extensive deep convection enhanced by the strong surface wind convergence areas in January 1984. Our results are consistent with those of Gutzler and Wood (1990), who find strong correlations between time series of OLR and surface wind convergence primarily in the east Pacific.

Figure 11 illustrates the relationship of DCC top temperatures to the SST distribution. Because of the small longitudinal temperature gradient in the middle and upper tropical troposphere (Oort 1983) we can simply relate cloud top altitudes to cloud top temperatures. Positive correlations between DCC top altitudes and SST are evident in the west Pacific in July 1983 (Fig. 11a) and the east Pacific in January 1984 (Fig. 11d). The correlation is much weaker or nonexistent in the east Pacific in July 1983 (Fig. 11b) and the west Pacific in January 1984 (Fig. 11c). The analysis of the first two years of ISCCP C1 data shows that there is in general a positive correlation between DCC top altitude and SST in both the west Pacific and east Pacific although the slope is larger in the west Pacific. Del Genio and Yao (1987), who analyzed a different version of the ISCCP data for the Atlantic Ocean, found that the peak of the DCC top distribution was highest (near 150 mb) in the west Atlantic, where the SST was a local maximum, and shifted toward lower levels as one moved eastward (to a lower SST area). DCC visible reflectances do not vary systematically with SSTs in either month. In July 1983, DCC reflectances were about the same in the west Pacific and east Pacific (≈ 0.75). In January 1984, DCC in the west Pacific (≈ 0.77) were marginally brighter than those in the east Pacific (≈ 0.75). The higher reflectance might be due to either greater fractional coverage of individual pixels by thick clouds, or to greater liquid water content in the convective clouds. In either case, this may be evidence of a strengthening Walker circulation following an El Niño event.

We tested the sensitivity of these results to spatial resolution by redoing the analysis with grid boxes of $2^{\circ} \times 6^{\circ}$, $4^{\circ} \times 4^{\circ}$ and $2^{\circ} \times 10^{\circ}$ latitude-longitude extent (the actual spatial resolution of the FSU wind data). The results at $2^{\circ} \times 6^{\circ}$ and $2^{\circ} \times 10^{\circ}$ resolutions are not significantly different from those at $2^{\circ} \times 2^{\circ}$ resolution. At $4^{\circ} \times 4^{\circ}$ resolution, there is a marginally significant increase in extensive deep convection in regime 8. This cannot be completely explained by the

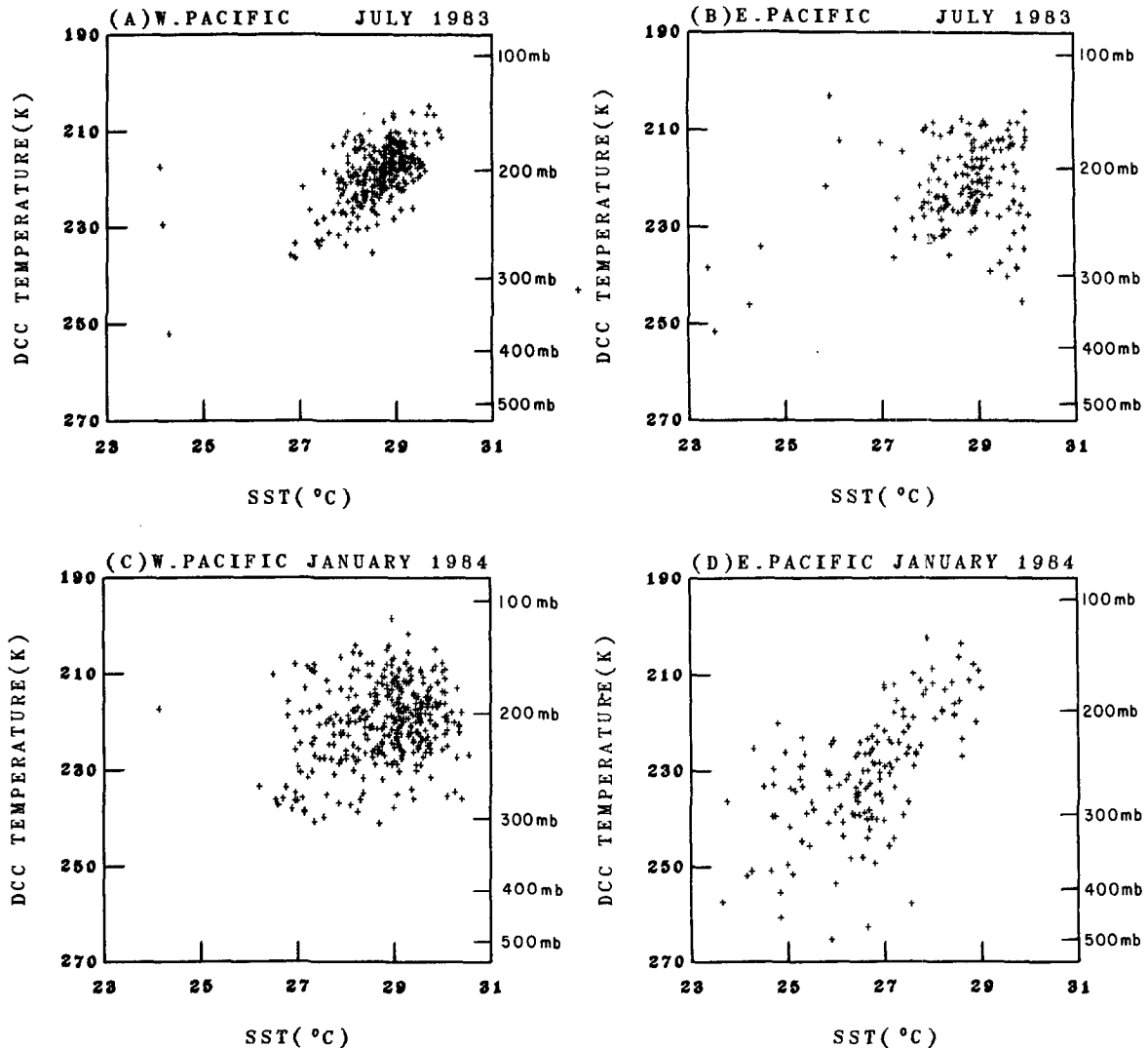


FIG. 11. Scatter plots of extensive deep convection as defined in the text as a function of DCC brightness temperature (altitude) and SST. The pressures plotted along the right edge of each panel are converted to altitude using the mean vertical temperature profile for 20°S – 20°N latitudinal range (Newell et al. 1973). (a) west Pacific, July 1983; (b) east Pacific, July 1983; (c) west Pacific, January 1984; (d) east Pacific, January 1984.

fact that the $4^{\circ} \times 4^{\circ}$ resolution tends to reduce the absolute value of divergence because the increase of the fraction of extensive deep convection ($\approx 15\%$) is much larger than that of the population of all data points ($\approx 5\%$) in regime 8 in July 1983. However, this change does not affect our conclusions. Sensitivity to the definition of extensive deep convection was tested by varying the cut-off value from 1% to 2% to 3%. This produces no statistically significant variation in the results.

6. Discussion

In Figs. 6 and 7, the latitudinal width of the ITCZ is about 5° (cf., Garcia 1985) which is some 10° nar-

rower than that suggested by OLR observations (Liebmann and Hartmann 1982). This may not be a problem for diagnosing signals of low-frequency, tropical phenomena, such as ENSO and the 40–50 day oscillation. However, this deficiency of OLR analyses may well be important in studying the dynamics of tropical air–sea interactions and in verification of cumulus parameterizations. The atmospheric circulation is sensitive to the geographic distribution of diabatic heating as well as its vertical distribution (cf., Hartmann et al. 1984; DeMaria 1985). The net diabatic heating includes contributions from clear sky, cumulus clouds, and mesoscale anvils, which have different magnitudes and different geographical and vertical distributions of radiative and latent heating (Houze 1982, 1989). In

particular the DCC might be better indicators of cumulus heating which predominates in the lower troposphere, while the CAC might indicate mesoscale anvil heating of the upper troposphere. The fact that the diurnal cycle of total precipitation at the surface is consistent with that of DCC rather than CAC suggests that DCC precipitation rates are much higher and thus, the intensity of latent heating in the convective complex is much higher in the DCC part. The larger areal coverage of CAC suggests that they have a stronger influence on radiative heating and cooling of the convective complex. Therefore, study of the processes that contribute to the net large-scale diabatic heating requires separate knowledge of DCC, CAC, and clear sky regions. The OLR pattern mixes at least DCC and CAC together, whereas the VS-IR method separates them.

The variations we see in the DCC-SST-surface wind convergence relationship raise the issue of differences in the predominant atmosphere-ocean coupling mechanism between the west Pacific and the east Pacific. Gutzler and Wood (1990) have suggested that the SST gradient may play an important role by kinematically forcing low-level atmospheric circulation anomalies over the east Pacific. We will attempt to address this issue from a slightly different angle.

The west Pacific type of relationship could be explained by the effect of SST on atmospheric instability⁸. Taking the vertical profiles of moist static energy (h) and saturation moist static energy (h^*) observed in the Marshall Islands (Lord and Arakawa 1980) as representative of the west Pacific, and assuming that a change of SST affects these profiles only below the level of minimum h^* (i.e., ignoring the influence of SST variation on the middle and upper troposphere), the atmosphere can be made convectively stable (h at the surface is less than the minimum h^*) with a 2°C decrease in SST. In other words, convection will be suppressed for SST less than 27°C if the typical SST in the Marshall Islands is 29°C (cf., Fig. 6a). Thus, simple thermodynamics might explain the critical SST for occurrence of deep convection in this regime. In areas of SST warmer than 28°C, the lack of correlation between deep convection and strong convergence also suggests an environment unstable enough, due to surface influences alone, for convection to occur without strong surface convergence.

The east Pacific type of relation suggests that low-level convergence, probably associated with SST gradients (Lindzen and Nigam 1987), may be more important. Although relatively cool SST (colder than 27°C) tends to stabilize the atmosphere near the surface, strong low-level convergence acts to destabilize the atmosphere above cloud base by adiabatic cooling

in the middle troposphere and by deepening the PBL. Thus, the difference between the west and east Pacific types may be a matter of whether convective stability is controlled primarily by thermodynamic, essentially one-dimensional processes near the surface (the west Pacific) or by thermodynamic and dynamic (i.e., at least two-dimensional) processes both near and above the surface (the east Pacific).

Because of the limitations of the data, our analysis cannot supply any evidence to explain the absence of enhanced DCC in areas of SST < 27°C with strong surface wind convergence in the west Pacific. However, it would be reasonable to speculate that extensive DCC occurring in the warmest SST areas stabilize adjacent areas via upper level subsidence and thus suppress occurrence of DCC in those areas in the west Pacific with SST < 27°C, despite strong surface wind convergence.

What causes the change from the west Pacific to the east Pacific type of relation? Garcia et al. (1986) constructed vertical profiles of equivalent potential temperature and saturation equivalent potential temperature in the tropical east Pacific for several time periods. Their results indicate that the atmosphere was convectively unstable during an El Niño winter (January 1983) and stable in a non-El Niño winter (November 1980). Thus, variations of the large-scale atmospheric circulation associated with SST variations could change the dynamic regime in the east Pacific. Our results for a non-El Niño winter (January 1984) indicate that most convective cloud tops in the east Pacific were relatively low (Figs. 2d, 11d). If convective heating was more confined to the lower troposphere at that time and place, a stronger feedback between convection and low-level wind convergence might be expected. Cumulus heating profiles for the west Pacific and east Atlantic show marked differences of this kind (Thompson et al. 1979).

A possible explanation of the DCC top temperature-SST relationship is that SST affects DCC top altitude by its influence on convective instability. Again taking observed vertical profiles of h and h^* for the Marshall Islands (Lord and Arakawa 1980), assuming that SST variations only affect h and h^* below the level of the minimum h^* , and fixing surface relative humidity at 78%, we get approximately a 1 km decrease in DCC altitude for a 2°C surface cooling, typical of the SST difference between convective areas of the west Pacific and east Pacific. This simple estimate agrees with our observations.

The DCC top temperature-SST relationship we see is suggestive of the tendency for convective clouds to deepen in GCM simulations of warmer climates. Although lapse rate and surface relative humidity variations also affect the penetration depth of convection, neither is likely to totally offset the effect of surface temperature changes. For example, for a 4°C surface warming, the lapse rate would have to increase by sev-

⁸ Betts and Ridgway (1989) gave a similar explanation based on the results of their convective boundary layer model.

eral times the change in the moist adiabatic lapse rate to cancel the increase in surface moist static energy. In the tropics, where moist convection controls the lapse rate, such a change can probably be ruled out on climatic time scales.

7. Summary

Previous studies inferring deep convection from satellites have not systematically isolated DCC from other high clouds that are associated with DCC. We have developed two methods to improve the detection of DCC from satellite images. Method 1 is a combined VS-IR threshold method which isolates DCC by adding VS channel information to the usual IR channel approach. Method 2 is an IR-only threshold method that is adjusted against method 1. Both methods prove capable of distinguishing DCC from other high clouds and provide generally consistent results. A detailed comparison of the two methods suggests that method 1 must be used to detect large-scale variations of DCC or CAC top altitudes. Method 2, on the other hand, must be adjusted by using method 1 results for different regions if there is a systematic difference of cloud top heights between these regions.

Using these two methods, we have examined the monthly mean spatial distribution of DCC in the tropical Pacific, the diurnal variation of DCC, and the relation of DCC to SST and surface wind convergence. Changes in the positions of the ITCZ and SPCZ between July 1983 and January 1984 appear to be related to both the waning El Niño and the normal seasonal cycle. The latitudinal extent of extensive deep convection is significantly smaller than that inferred from analysis of OLR. DCC top temperature was about 8 K warmer (≈ 1 km lower in altitude) in the east Pacific than in the west Pacific in January 1984, suggesting the possible influence of the large-scale Walker circulation. In July 1983, DCC top temperature was about the same in the west Pacific and the east Pacific, which may be an indication of the relaxation of the Walker circulation.

The diurnal variation of DCC over ocean indicates that DCC amount at local noon is a good representation of the daily mean with less than 10% over- or under-estimate of daily means. The relative amplitude of the diurnal cycle of DCC amount (20%–40%) is stronger than that of the associated mesoscale CAC (10%–20%), but the reverse is true for the absolute amplitudes. DCC cover peaks in the early morning throughout the equatorial Pacific, while mesoscale CAC cover peaks in late afternoon. The maximum amplitude of the diurnal cycle occurs in the west Pacific or Indonesia, where deep convection is most intense. The consistency of diurnal variations between DCC and precipitation suggests that DCC dominate the variation of precipitation. DCC top temperatures are a minimum near or several hours before the maximum in DCC

cover and are out of phase with mesoscale CAC top temperatures.

Our results suggest that monthly mean deep convection does not consistently correlate with monthly mean evaporation. When the warmest SSTs in a particular subregion of the tropical Pacific are greater than 28°C over a substantial area, DCC are enhanced only where $\text{SST} > 28^{\circ}\text{C}$ in the absence of strong surface wind divergence. This occurs at most times in the west Pacific and in the east Pacific during El Niño and northern summer months. Moreover, in places where $\text{SST} < 28^{\circ}\text{C}$, although the colocated monthly mean surface wind is usually divergent, the few areas of strong convergence do not contain enhanced deep convection. When the warmest SSTs in a subregion are less than about 28°C , deep convection exhibits a preference for areas of strong monthly mean surface wind convergence, such as in the east Pacific in non-El Niño, non-summer months. Our results suggest that the transition between the two types of relationship is related primarily to the area covered by $\text{SST} > 28^{\circ}\text{C}$. Consideration of the typical vertical structure of the tropical atmosphere suggests that this difference in behavior may reflect control of convective stability by surface vs. midtropospheric processes, consistent with the positive correlation of DCC top altitude and SST.

Although the time period examined here is too short to study the climatological features of DCC, certain aspects of the nature of tropical deep convection are supported by a two year analysis of a different version of the ISCCP data. A more extensive database is required in particular to test our assertion that the deep convection/SST/convergence relationship is controlled by the maximum SST in a specific region and month. The planned 12-year duration of ISCCP will permit such a study using the techniques we have developed. Our diagnosis of the processes producing the DCC variations is limited by the absence of accurate global datasets of low-level winds, moisture, air temperature and PBL height. Simultaneous information on all these parameters represents our best hope for understanding tropical deep convection and its effect on the large scale circulation in the tropics.

Acknowledgments. The authors are grateful to Mark Cane for extensive suggestions and for providing the SST and wind data. Special thanks to Inez Fung, David Rind, Stephen Zebiak, Richard Seager and Qing-Yuan Han for constructive discussion and helpful comments on the manuscript. We also thank Shu-Pui Chan and Patrice Palmer for their help with programming and photographs. We appreciate the thoughtful comments of David Gutzler and an anonymous reviewer. This research was supported by the NASA Climate Program.

REFERENCES

- Adler, R. F., and A. J. Negri, 1988: A satellite infrared technique to estimate tropical convective and stratiform rainfall. *J. Climate Appl. Meteor.*, **27**, 30–51.

- Albright, M. D., E. E. Recker and R. J. Reed, 1985: The diurnal variation of deep convection and inferred precipitation in the central tropical Pacific during January–February 1979. *Mon. Wea. Rev.*, **113**, 1663–1680.
- Ardanuy, P. E., and H. L. Kyle, 1986: El Niño and outgoing longwave radiation: Observations from Nimbus-7 ERB. *Mon. Wea. Rev.*, **114**, 415–433.
- Arkin, P. A., and P. E. Ardanuy, 1989: Estimating climatic-scale precipitation from space: A review. *J. Climate*, **2**, 1229–1238.
- Bjerknes, J., 1969: Atmospheric teleconnections from the equatorial Pacific. *Mon. Wea. Rev.*, **97**, 163–172.
- Brest, C. L., and W. B. Rossow, 1990: Radiometric calibration and monitoring of NOAA AVHRR data for ISCCP. *Int. J. Remote Sens.*, in press.
- Cornejo-Garrido, A. G., and P. H. Stone, 1977: On the heat balance of the Walker circulation. *J. Atmos. Sci.*, **34**, 1155–1162.
- Crutcher, H. L., and J. M. Meserve, 1970: Selected level heights, temperatures and dew points for the northern hemisphere. NA-VAIR 50-1C-52, 424 pp. [U.S. Govt. Printing Office]
- Del Genio, A. D., and M. S. Yao, 1987: Properties of deep convective clouds in the ISCCP pilot data set. Preprints, *17th Conf. on Hurricanes and Tropical Meteorology*, Miami, Amer. Meteor. Soc., 133–136.
- , and —, 1988: Sensitivity of a global climate model to the specification of convective updraft and downdraft mass fluxes. *J. Atmos. Sci.*, **45**, 2641–2668.
- DeMaria, M., 1985: Linear response of a stratified tropical atmosphere to convective forcing. *J. Atmos. Sci.*, **42**, 113–121.
- Finkelstein, J., 1964: Diurnal variation of rainfall amount on tropical Pacific islands. *Symp. on Tropical Meteor., Rotorua, N.Z., Proc. New Zealand Meteorology Services*, Wellington, 286–294.
- Garcia, O., 1985: Atlas of highly reflective clouds for the global tropics: 1971–1983. Environ. Res. Lab., Natl. Oceanic and Atmos. Admin., Boulder, 365 pp.
- , S. J. S. Khalsa and E. J. Steiner, 1986: Atmospheric characteristics of the equatorial Pacific during the 1982–1983 El Niño, deduced from satellite and aircraft observations. *J. Geophys. Res.*, **91**, 13217–13231.
- Goldenberg, S. B., and J. J. O'Brien, 1981: Time and space variability of tropical Pacific wind stress. *Mon. Wea. Rev.*, **109**, 1190–1206.
- Graham, N., and T. P. Barnett, 1987: Observations of sea surface temperature and convection over tropical oceans. *Science*, **238**, 657–659.
- Gray, W. M., and R. W. Jacobson, Jr., 1977: Diurnal variation of deep convection. *Mon. Wea. Rev.*, **105**, 1171–1188.
- Gutzler, D. S., and T. M. Wood, 1990: Structure of large-scale convective anomalies over tropical oceans. *J. Climate*, **3**, 483–496.
- Hansen, J., A. Lacis, D. Rind, G. Russell, P. Stone, I. Fung, R. Ruedy and J. Lerner, 1984: Climate sensitivity: Analysis of feedback mechanisms. *Climate Processes and Climate Sensitivity, Geophysical Monograph 29*, Maurice Ewing Volume 5, 130–163.
- Hartmann, K. L., H. H. Hendon and R. A. Houze, Jr., 1984: Some implications of the mesoscale circulations in tropical cloud clusters for large-scale dynamics and climate. *J. Atmos. Sci.*, **41**, 113–121.
- Hartmann, D. L., and E. E. Recker, 1986: Diurnal variation of outgoing longwave radiation in the tropics. *J. Climate Appl. Meteor.*, **25**, 800–812.
- Heddinghaus, T. R., and A. F. Krueger, 1981: Annual and interannual variations in outgoing longwave radiation over the tropics. *Mon. Wea. Rev.*, **109**, 1208–1218.
- Houze, Jr., R. A., 1982: Cloud clusters and large-scale vertical motions in the tropics. *J. Meteorol. Soc. Jpn.*, **60**, 396–409.
- , 1989: Observed structure of mesoscale convective systems and implications for large-scale heating. *Quart. J. Roy. Meteor. Soc.*, **115**, 425–461.
- , and A. K. Betts, 1981: Convection in GATE. *Rev. Geophys. Space Phys.*, **19**, 541–576.
- Hsiung, J., 1986: Mean surface energy fluxes over the global ocean. *J. Geophys. Res.*, **91**, 10 585–10 606.
- Johnson, R. H., 1980: Diagnosis of convective and mesoscale motions during phase III of GATE. *J. Atmos. Sci.*, **37**, 733–753.
- Julian, P. R., and R. M. Chervin, 1978: A study of the Southern Oscillation and Walker circulation phenomenon. *Mon. Wea. Rev.*, **106**, 1433–1451.
- Khalsa, S. J. S., 1983: The role of sea surface temperature in large-scale air–sea interaction. *Mon. Wea. Rev.*, **111**, 954–966.
- Lambert, S., 1988: A comparison of operational global analyses from the European Centre for Medium Range Weather Forecasts (ECMWF) and the National Meteorological Center (NMC). *Tellus*, **40A**, 272–284.
- Lau, K. M., and P. H. Chan, 1983a: Short-term climate variability and atmospheric teleconnections from satellite-observed outgoing longwave radiation. Part I: Simultaneous relationships. *J. Atmos. Sci.*, **40**, 2735–2750.
- , and —, 1983b: Short-term climate variability and atmospheric teleconnections from satellite-observed outgoing longwave radiation. Part II: Lagged correlations. *J. Atmos. Sci.*, **40**, 2751–2767.
- , and —, 1985: Aspects of the 40–50 day oscillation during the northern winter as inferred from outgoing longwave radiation. *Mon. Wea. Rev.*, **113**, 1889–1908.
- , and S. H. Shen, 1988: On the dynamics of intraseasonal oscillations and ENSO. *J. Atmos. Sci.*, **45**, 1781–1797.
- Liebmann, B., and D. L. Hartmann, 1982: Interannual variation of outgoing IR associated with tropical circulation changes during 1974–78. *J. Atmos. Sci.*, **39**, 1153–1162.
- Lindzen, R. S., and S. Nigam, 1987: On the role of sea surface temperature gradients in forcing low level winds and convergence in the tropics. *J. Atmos. Sci.*, **44**, 2418–2435.
- Liou, K. N., 1976: On the absorption, reflection and transmission of solar radiation in cloudy atmospheres. *J. Atmos. Sci.*, **33**, 798–805.
- Liu, W. T., 1988: Moisture and latent heat flux variabilities in the tropical Pacific derived from satellite data. *J. Geophys. Res.*, **93**, 6749–6760.
- Lord, S. J., and A. Arakawa, 1980: Interaction of a cumulus cloud ensemble with the large-scale environment. Part II. *J. Atmos. Sci.*, **37**, 2677–2691.
- Meehl, G. A., 1987: The annual cycle and interannual variability in the tropical Pacific and Indian Ocean regions. *Mon. Wea. Rev.*, **115**, 27–50.
- Meisner, B. N., and P. A. Arkin, 1987: Spatial and annual variations in the diurnal cycle of large-scale tropical convection cloudiness and precipitation. *Mon. Wea. Rev.*, **115**, 2009–2032.
- Minnis, P., and E. F. Harrison, 1984: Diurnal variability of regional cloud and clear-sky radiative parameters derived from GOES data. Part I: Analysis method. *J. Climate Appl. Meteor.*, **23**, 993–1011.
- , and G. G. Gibson, 1987: Cloud cover over the equatorial eastern Pacific derived from July 1983 International Satellite Cloud Climatology Project data using a hybrid bispectral threshold. *J. Geophys. Res.*, **92**, 4051–4078.
- Murakami, T., 1980: Empirical orthogonal function analysis of satellite-observed outgoing longwave radiation during summer. *Mon. Wea. Rev.*, **108**, 205–222.
- , 1983: Analysis of the deep convective activity over the western Pacific and Southeast Asia. Part I: Diurnal variation. *J. Meteorol. Soc. Jpn.*, **61**, 60–75.
- Neelin, J. D., I. M. Held and K. H. Cook, 1987: Evaporation-wind feedback and low-frequency variability in the tropical atmosphere. *J. Atmos. Sci.*, **44**, 2341–2348.
- Nitta, T., 1986: Long-term variations of cloud amount in the western Pacific region. *J. Meteorol. Soc. Jpn.*, **64**, 373–389.
- Newell, R. E., J. W. Kidson, D. G. Vincent and G. J. Boer, 1973: *The Circulation of the Tropical Atmosphere and Interactions with Extratropical Latitudes*. Vol. 1, Massachusetts Institute of Technology press, 258 pp.
- Ogura, Y., and H. R. Cho, 1973: Diagnostic determination of cumulus

- cloud populations from observed large-scale variables. *J. Atmos. Sci.*, **30**, 1276–1286.
- Oort, A. H., 1983: *Global Atmospheric Circulation Statistics, 1958–1973*. NOAA Prof. Pap. 14, NOAA Geophysical Fluid Dynamics Laboratory, U.S. Dept. of Commerce, 180 pp.
- Reed, R. J., and E. E. Recker, 1971: Structure and properties of synoptic-scale wave disturbances in the equatorial western Pacific. *J. Atmos. Sci.*, **28**, 1117–1133.
- Reynolds, R. W., 1983: A comparison of sea surface temperature climatologies. *J. Climate Appl. Meteor.*, **22**, 447–458.
- Riehl, H., and J. S. Malkus, 1958: On the heat balance in the equatorial trough zone. *Geophysica*, **6**, 503–538.
- Rossow, W. B., A. A. Lacis and P. J. Lu, 1990: Global seasonal cloud and radiation balance variations from satellite radiance measurements. *J. Climate*, in press.
- , E. Kinsella, A. Wolf and L. Garder, 1987: *International Satellite Cloud Climatology Project (ISCCP) Description of Reduced Resolution Radiance Data*. WMO/TD-No. 58 (Revision), World Climate Research Programme (ICSU/WMO), 143 pp.
- , L. C. Garder, P. J. Lu and A. Walker, 1988: *International Satellite Cloud Climatology Project (ISCCP) Documentation of Cloud Data*. WMO/TD-No. 266, World Climate Research Program (ICSU/WMO), 75 pp. plus two appendices.
- Rowntree, P. R., 1972: The influence of tropical east Pacific Ocean temperature on the atmosphere. *Quart. J. Roy. Meteor. Soc.*, **98**, 290–321.
- Sarachik, E., 1980: Review of cloud generation in climate models. *Clouds in Climate: Modeling and Satellite Observational Studies*, Report of Workshop held at NASA Goddard Institute for Space Studies, 222 pp.
- Scheaffer, R. L., and J. T. McClave, 1982: *Statistics for Engineers*. Duxbury Press, 475 pp.
- Schiffer, R. A., and W. B. Rossow, 1985: ISCCP global radiance data set: A new resource for climate research. *Bull. Amer. Meteor. Soc.*, **66**, 1498–1505.
- Schlesinger, M. E., and D. L. Mitchell, 1987: Climate model simulations of the equilibrium climatic response to increased carbon dioxide. *Rev. Geophys.*, **25**, 760–798.
- Sèze, G., and W. B. Rossow, 1990: Time-cumulated visible and infrared radiance histograms used as descriptors of surface and cloud variations. *Int. J. Remote Sens.*, in press.
- Simmons, A. J., 1982: The forcing of stationary wave motion by tropical diabatic heating. *J. Roy. Meteor. Soc.*, **108**, 503–534.
- Smith, S. D., and E. G. Banke, 1975: Variation of the sea surface drag coefficient with wind speed. *Quart. J. Roy. Meteor. Soc.*, **101**, 665–670.
- Steiner, E. J., 1987: The relationship of low-level winds and moisture to convection in the tropical Pacific. *Mon. Wea. Rev.*, **115**, 744–749.
- Stephens, G. L., 1978: Radiation profiles in extended water clouds. I: Theory. *J. Atmos. Sci.*, **35**, 2111–2132.
- Steranka, J., E. B. Rodgers and R. C. Gentry, 1984: The diurnal variation of Atlantic Ocean tropical cyclone cloud distribution inferred from geostationary satellite infrared measurements. *Mon. Wea. Rev.*, **112**, 2338–2343.
- Stowe, L. L., C. G. Wellemeier, T. F. Eck, H. Y. M. Yeh and the Nimbus-7 Cloud Data Processing Team, 1988: Nimbus-7 global cloud climatology. Part I: Algorithms and validation. *J. Climate*, **1**, 445–470.
- Thompson, R. M., Jr., S. W. Payne, E. E. Recker and R. J. Reed, 1979: Structure and properties of synoptic-scale wave disturbances in the intertropical convergence zone of the eastern Atlantic. *J. Atmos. Sci.*, **36**, 53–72.
- Webster, P. J., and G. L. Stephens, 1980: Tropical upper-tropospheric extended cloud: inferences from winter MONEX. *J. Atmos. Sci.*, **37**, 1521–1541.
- Wetherald, R. T., and S. Manabe, 1988: Cloud feedback processes in a general circulation model. *J. Atmos. Sci.*, **45**, 1397–1415.
- Whitlock, C. H., W. F. Staylor, G. Smith, R. Levin, R. Frouin, C. Gautier, P. M. Teillet, P. N. Slater, Y. J. Kaufman, B. N. Holben, W. B. Rossow, C. L. Brest and S. R. LeCroy, 1990: AVHRR and VISSR satellite instrument calibration results for both cirrus and marine stratus IFO periods. *FIRE Science Team Meeting*, Vail CO, July 1988. *NASA Conference Proceedings*, in press.
- Zebiak, S., 1990: Diagnostic studies of Pacific surface winds. *J. Climate*, (in press).
- Zipser, E. J., 1977: Mesoscale and convective-scale downdrafts as distinct components of squall-line circulation. *Mon. Wea. Rev.*, **105**, 1568–1589.
- , R. J. Meitin and M. A. LeMone, 1980: Cumulonimbus vertical velocity events in GATE, II: synthesis and model core structure. *J. Atmos. Sci.*, **37**, 2458–2469.